

Scattering by linear defects in graphene: a tight-binding approach

J. N. B. Rodrigues¹, N. M. R. Peres², and J. M. B. Lopes dos Santos¹

¹ CFP and Departamento de Física e Astronomia, Faculdade de Ciências
Universidade do Porto, P-4169-007 Porto, Portugal

² Physics Department and CFUM, University of Minho, P-4710-057, Braga, Portugal

E-mail: peres@fisica.uminho.pt

Abstract. We develop an analytical scattering formalism for computing the transmittance through periodic defect lines within the tight-binding model of graphene. We first illustrate the method with a relatively simple case, the *pentagon only* defect line. Afterwards, more complex defect lines are treated, namely the *zz(558)* and the *zz(5757)* ones. The formalism developed, only uses simple tight-binding concepts, reducing the problem to matrix manipulations which can be easily worked out by any computational algebraic calculator.

PACS numbers: 81.05.ue, 72.80.Vp

1. Introduction

Grain boundaries (GBs) in artificially grown solids are, most likely, unavoidable. This is particularly true for solids grown by chemical vapor deposition. In this method, the crystal starts growing simultaneously at different locations on the substrate. The relative orientations of the domains have a stochastic distribution and when two domains growing at different locations approach each other they form a GB.

If the grown crystal is used in a device larger than the size of the grains, then an electron has to pass through one or several GBs as it makes its way across the device. Therefore, the scattering problem of an electron off a GB becomes technologically relevant.

In low dimensional systems, such as graphene [1], the study of GBs is an active field of research [2, 3] and it has been shown that this type of disorder has a strong impact in the transport properties of graphene [4, 5, 6]. Indeed, one-dimensional defect lines can give rise to exotic effects, such as a valley filter [7, 8], where states from one Dirac cone are filtered from those belonging to the other inequivalent cone. It has been suggested that GBs can be exploited for novel graphene-based nanomaterials and functional devices [6].

The study of scattering by extended defects is revealing itself of increasing interest, specially after the recent work [9] by Tsen *et al.*. In the latter, using chemical vapor deposited polycrystalline graphene, the authors made electric measurements across a single GB. In this way, they were able to measure the electronic properties of single GBs. Tsen *et al.* have found that the transport properties of these systems are strongly dependent on their microscopic details. Each CVD synthesis method, typically gives rise to GBs with similar resistivity profiles. But the GBs originating from different synthesis procedures are normally very distinct. All this highlights the importance of the studies presented on this paper concerning the electronic properties of defect lines in graphene.

The study of one localized impurity in a one-dimensional system has a simple analytical solution [10], which was later generalized to the ladder case [11]. This method is, however, inappropriate for tackling more complex systems. For problems of the same nature as the ones considered in this work, the method of non-equilibrium Green's functions is often employed [7, 12]. Unfortunately, such method is not so easy to follow by the non-specialist, although there is a one-to-one correspondence between the Green's function method and the mode matching one [13]. A more elementary method, based on the work of Ando [14], was applied to the solution of a defect on ultra-narrow graphene [15]. Here we develop an approach, with close resemblance to the method of Ando for quantum point contacts, which is particularly suitable to deal with extended periodic defects. Its starting point is the reduction of the two-dimensional scattering problem to an effective quasi-one-dimensional one, whose solution is simpler to work out.

In the context of the first-neighbor tight-binding model of graphene, we study the electronic scattering from periodic defect line in graphene, developing a systematic procedure to approach such problems. We illustrate the method with three types of defect lines oriented along the zigzag direction. In a companion paper we have focused on the continuum low-energy limit of the electronic scattering from the defect lines under study in the present text [16].

In Section 2 we start by describing briefly and in general terms how these kind of problems can be tackled. After that introduction, we concentrate on the study of electron scattering from a simple model of a defect line on graphene, namely the *pentagon-only* defect line (Section 3). We then analyze two more complex defect lines, namely the $zz(5757)$ [16] and the $zz(558)$ ones [17, 8, 7, 16] (see Section 4). Finally, in Section 5 we summarize the results obtained and pinpoint the strengths of the method presented in this paper.

2. General formulation of the problem

Electronic scattering from periodic extended defects in the center of a pristine 2D crystal is essentially equivalent to the electron scattering from a localized defect at the center of a quasi-1D crystal. Such a statement arises from the fact that the periodic extended defect preserves crystal's translation invariance along the defect direction. Therefore, we can Fourier transform the 2D crystal along the latter direction thus converting the

2D problem into a quasi-1D equivalent one.

Thereupon, this class of 2D problems can be treated under the framework of scattering 1D problems. Accordingly, in the present section we describe, with some generality, how one can work out electron scattering from a defect located at the center of a quasi-1D crystal modeled by a first neighbor tight-binding (TB) model (see Fig. 1). This will be the starting point for the treatment of some 2D scattering problems in graphene (see Sections 3 and 4).

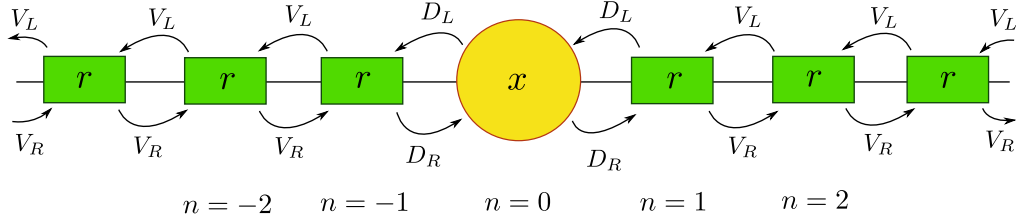


Figure 1. (Color online) Scheme of a general quasi-1D crystal with a defect at position $n = 0$. The unit cell in the bulk (green rectangles), encompasses r Wannier states, while in the defect (yellow circumference) there are x states. The generalized hopping amplitude V_L ($V_R = V_L^\dagger$), is a matrix that contains all the hopping amplitudes between Wannier states of neighbor bulk unit cells. The generalized hopping amplitude D_L (D_R), is a $x \times r$ matrix containing the hopping amplitudes connecting all the Wannier states in the defect and those in the unit cell at $n = -1$ ($n=1$).

We start by writing the TB bulk equations of the general quasi-1D crystal with a defect at its center (see Fig. 1). Away from the defect, these can be cast in the form

$$V_R \mathbf{c}(n-1) + (H - \epsilon \mathbb{I}_r) \mathbf{c}(n) + V_L \mathbf{c}(n+1) = 0. \quad (1)$$

In Eq. (1), \mathbf{c} stands for a column vector with as many entries as there are Wannier states in the quasi-1D crystal's unit cell; we denote this number by r . Therefore, the terms H , \mathbb{I}_r , V_L and V_R are $r \times r$ matrices, \mathbb{I}_r standing for the unit matrix. The matrix H describes the hopping processes occurring inside the unit cell, while V_L (V_R) describes the hopping processes occurring between the unit cell at position n and the unit cell at position $n+1$ ($n-1$). The hermitian nature of the Hamiltonian requires that $V_R = V_L^\dagger$.

The TB bulk equation [Eqs. (1)] can usually be written in a different form, where the amplitudes of the unit cell located at position $n+1$ are expressed in terms of the amplitudes of the unit cells located at positions n and $n-1$,

$$\mathbf{c}(n+1) = \mathbb{T}_1 \mathbf{c}(n) + \mathbb{T}_2 \mathbf{c}(n-1), \quad (2)$$

where \mathbb{T}_i are $r \times r$ matrices, which we call transfer matrices. These matrices are generally non-hermitian. Usually Eq. (2) cannot be obtained directly from Eq. (1) for site n , because the matrix V_L is not invertible. However, for the cases of interest, we can in general obtain Eq. (2) from the TB equations [Eq. (1)] for the sites n and $n+1$. When the one-dimensional chain is AB -like (see Fig. 2) the transfer matrix description further simplifies to

$$\mathbf{c}(n+1) = \mathbb{T} \mathbf{c}(n), \quad (3)$$

where there is now only one transfer matrix \mathbb{T} relating neighbor amplitudes. Since in the present text we are specially interested in studying graphene crystals, whose Fourier transformed systems give rise to AB -like chains, we will from now on simplify our analysis by assuming that our general 1D chain is described by a relation of the form of Eq. (3).

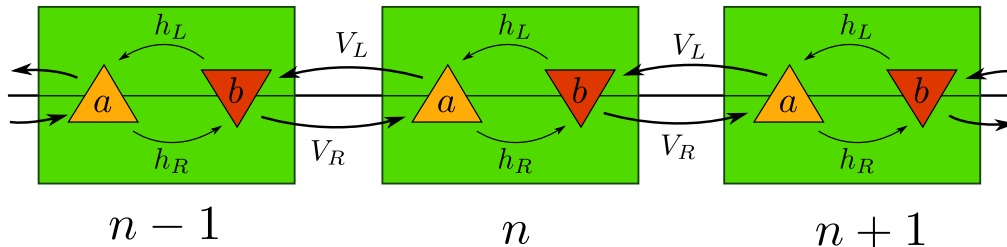


Figure 2. (Color online) Scheme of a general quasi-1D AB crystal. The unit cell of the crystal (green rectangles) encompasses $r = a + b$ Wannier states. The generalized hopping amplitude V_L ($V_R = V_L^\dagger$), is a matrix that contains all the hopping amplitudes between Wannier states of neighboring unit cells. These generalized hopping amplitudes, are only non-zero when connecting the a and b Wannier states of different unit cells. In contrast, they are zero both between the a Wannier states of two neighboring unit cells, and between b Wannier states of neighboring unit cells.

Inherent to the study of any scattering problem is the determination of the transverse propagating (or evanescent) modes allowed in the system. In the case of a one-dimensional periodic chain the computation of the modes can be done using Bloch's theorem. In that prescription, we write the amplitudes at position $n+1$ and $n-1$ in terms of those at position n : $\mathbf{c}(n+1) = e^{ik_j a} \mathbf{c}(n) \equiv \lambda_j \mathbf{c}(n)$ and $\mathbf{c}(n-1) = e^{-ik_j a} \mathbf{c}(n) \equiv \mathbf{c}(n)/\lambda_j$, where k_j stands for the wave-number along the chain direction associated with the mode indexed by j , and a stands for the length of the primitive vector. Using these relations, we can rewrite Eq. (1) as

$$\frac{1}{\lambda_j} V_R \mathbf{c}(n) + (H - \epsilon \mathbb{I}_r) \mathbf{c}(n) + \lambda_j V_L \mathbf{c}(n) = 0. \quad (4)$$

The r eigenvalues $\lambda_j = e^{ik_j a}$ and their r associated eigenvectors $|\psi_j\rangle$ permitted at a given energy ϵ , are obtained by solving this generalized eigenproblem. On the other hand, when one is able to write the TB equations in the form of a recurrence relation of the form of Eq. (3), it becomes obvious that the λ_j and $|\psi_j\rangle$ are, respectively, the eigenvalues and right eigenvectors of the transfer matrix, \mathbb{T} .

Let us now turn our attention to the defect, so that we can determine the boundary condition that the modes should satisfy when scattering from it. We start by assuming that regardless of the complexity of the defect at the center of the 1D crystal, the latter is located at position $n = 0$ (see Fig. 1). Therefore, the TB equations associated with the amplitudes at the defect can be generally written as

$$D_R \mathbf{c}(-1) + (H_D - \mathbb{I}_r) \mathbf{d}(0) + D_L \mathbf{c}(1) = 0. \quad (5)$$

In the above equation, D_L (D_R) is a $x \times r$ rectangular matrix containing all possible hopping amplitudes connecting the defect Wannier states and those of the unit cell

located at position $n = +1$ ($n = -1$). The matrix H_D encompasses all the hopping amplitudes between the x Wannier states of the defect, whose amplitudes are grouped in the x -dimensional array $\mathbf{d}(0)$. Note that Eq. (5) is a shorthand for a system of equations, containing x TB equations associated with the x states at the defect and $x + 2r$ unknown amplitudes. As a consequence, if we want to write a passage equation relating the amplitudes at $\mathbf{c}(1)$ and those at $\mathbf{c}(-1)$, we will also have to use the TB equations at position $n = -1$

$$V_R \mathbf{c}(-2) + (H - \mathbb{I}_r) \mathbf{c}(-1) + D_L \mathbf{d}(0) = 0, \quad (6)$$

as well as the transfer matrix relation $\mathbf{c}(-1) = \mathbb{T} \mathbf{c}(-2)$. Doing so, we end up with $x + 3r$ unknown amplitudes and $x + 2r$ equations. We choose to solve them by expressing $\mathbf{c}(1)$, $\mathbf{d}(0)$ and $\mathbf{c}(-2)$ ($x + 2r$ amplitudes) in terms of $\mathbf{c}(-1)$. Therefore, we will be able to write a passage equation relating the amplitudes before and after the defect as

$$\mathbf{c}(1) = \mathbb{M} \mathbf{c}(-1), \quad (7)$$

where \mathbb{M} is a $r \times r$ matrix. It is natural to interpret the latter matrix as a boundary condition matrix imposed by the defect on the wave function at each one of its sides.

We have so far shown how one can determine both the scattering modes of the one-dimensional chain and the boundary condition they must obey at the defect. The only step remaining is the computation of the scattering coefficients. Let us suppose that we have an incoming mode from $n = -\infty$. We then expect to have both transmitted modes outgoing to $n = +\infty$ and reflected modes outgoing to $n = -\infty$. As a consequence, we can write the wave function at each side of the defect as

$$|\Psi(n) = |\Psi^L(n)\rangle \equiv \lambda_{i>}^{n+1} |\psi_i^>\rangle + \sum_{j=1}^{r_{<}} \rho_{ij} \lambda_{j<}^{n+1} |\psi_j^<\rangle, \quad \text{for } n \leq -1 \quad (8a)$$

$$|\Psi(n)\rangle = |\Psi^R(n)\rangle \equiv \sum_{j=1}^{r_{>}} \tau_{ij} \lambda_{j>}^{n-1} |\psi_j^>\rangle, \quad \text{for } n \geq 1 \quad (8b)$$

where the superscript L stands for the wave function to the *left* of the defect ($n < 0$), while the superscript R stands for the wave function to the *right* of the defect ($n > 0$). In Eqs. (8), the sum over j up to $r_{>}$ ($r_{<}$) stands for a sum over all the $p_{>}$ ($p_{<}$) propagating modes moving in the direction of $n = +\infty$ ($n = -\infty$) and all the $s_{>}$ ($s_{<}$) evanescent modes, decreasing (increasing) with increasing n . Note that the total number of propagating and evanescent modes must add up to r , the total number of modes: $r = r_{>} + r_{<} = p_{>} + s_{>} + p_{<} + s_{<}$, which in the AB chain happens to be equal to the number of Wannier states in the unit cell. Moreover, the coefficients ρ_{ij} (τ_{ij}) stand for the reflection (transmission) coefficients of the modes indexed by j for an incoming mode i .

Before proceeding, let us emphasize that in this text, we are going to use interchangeably two types of notation: we will use the vectorial notation when referring to the arrays of amplitudes at a given unit cell located at position n [see Eqs. (1)-(7)]; the Dirac *ket* notation will be used when referring to the eigenmodes of the one-dimensional chain, as well as to the wave function at a given position n [see Eqs. (8)].

As long as we know the mathematical expressions for the modes of the quasi-one-dimensional chain, $|\psi_j^>\rangle$ and $|\psi_j^<\rangle$, and the boundary condition matrix \mathbb{M} , the determination of the scattering coefficients in Eqs. (8), ρ_{ij} and τ_{ij} , is a straightforward calculation.

If we define a matrix U , with columns which are the r transverse modes

$$U = \left[|\psi_1^>\rangle, \dots, |\psi_{r>}^>\rangle, |\psi_1^<\rangle, \dots, |\psi_{r<}^<\rangle \right], \quad (9)$$

and the following two vectors,

$$|\Phi^L(n)\rangle = \left[0, \dots, 0, \lambda_{i>}^{n+1}, 0, \dots, 0, \rho_{i1} \lambda_{1<}^{n+1}, \dots, \rho_{ir<} \lambda_{r<}^{n+1} \right]^T, \quad (10a)$$

$$|\Phi^R(n)\rangle = \left[\tau_{i1} \lambda_{1>}^{n-1}, \dots, \tau_{ir>} \lambda_{r>}^{n-1}, 0, \dots, 0 \right]^T, \quad (10b)$$

it is clear that

$$|\Psi^L(n)\rangle \equiv U|\Phi^L(n)\rangle, \quad (11a)$$

$$|\Psi^R(n)\rangle \equiv U|\Phi^R(n)\rangle. \quad (11b)$$

The passage equation, 7, then becomes

$$|\Phi^R(1)\rangle = U^{-1}\mathbb{M}U|\Phi^L(-1)\rangle. \quad (12)$$

This is a non-homogeneous system of r linear equations with r unknowns, $\rho_{i1}, \dots, \rho_{ir<}$ and $\tau_{i1}, \dots, \tau_{ir>}$, which we solve to obtain these scattering amplitudes.

When carrying out these calculations in a computer algebra system, the following remark may be useful. Since the transfer matrix is non-hermitian, its eigenbasis is not orthogonal. Nevertheless we can define a dual basis $|\tilde{\psi}_j\rangle$, $j = 1, \dots, r$ by the relation

$$\langle \tilde{\psi}_j | \psi_i \rangle = \delta_{ij} \quad (13)$$

and it is clear that the matrix U^{-1} j^{th} row is just the vector $\langle \tilde{\psi}_j |$, seen that the i^{th} column of U is $|\psi_i\rangle$; in the Appendix A, we show that these vectors $\langle \tilde{\psi}_j |$ can be simply obtained as the right eigenvectors of the transpose of the transfer matrix \mathbb{T}^T .

It is worth noting that the boundary condition arising from the presence of the defect, Eq. (7), must conserve the particle current (see Appendix B). Equivalently, the current on the left hand side of the defect, $\mathcal{J}_L \equiv \mathcal{J}(-1) = \langle \psi(-1) | \hat{\mathcal{J}} | \psi(-1) \rangle$, must be equal to the current on the right hand side of the defect, $\mathcal{J}_R \equiv \mathcal{J}(1) = \langle \psi(1) | \hat{\mathcal{J}} | \psi(1) \rangle$, where $\hat{\mathcal{J}}$ stands for the current operator. Therefore, the boundary condition matrix, \mathbb{M} , must satisfy the following equality

$$\mathbb{M}^\dagger \cdot \hat{\mathcal{J}} \cdot \mathbb{M} = \hat{\mathcal{J}}. \quad (14)$$

In the following sections we solve three electronic scattering problems using the machinery just presented. We will see that it simplifies the mathematical treatment of such problems without leading to a substantial loss of physical insight and intuition over the physical phenomena going on. On one hand, using the transfer matrix formalism we are able to write the scattering modes $\lambda_j |\psi_j\rangle = e^{ik_j a} |\psi_j\rangle$ directly in terms of the energy ϵ and the wave-number along the defect line, k_x . We thus avoid to write the

former in terms of the wave-number perpendicular to the defect line, $\mathbf{k} \cdot \mathbf{u}_2$. On the other hand, the described procedure allows us to compute an expression relating the TB amplitudes at the two sides of the defect. This has the obvious interpretation as being the boundary condition imposed on the wave function at the defect. As we will see in Sections 3 and 4, such a boundary condition relation can be obtained after some simple algebraic manipulations of the TB equations at the defect.

With this in mind, let us now apply this formalism to three types of zigzag oriented defect lines in graphene: the *pentagon-only* defect line (see Fig. 3), the *zz(5757)* defect line (see left panel of Fig. 7) and the *zz(558)* defect line (see right panel of Fig. 7).

3. Scattering from a *pentagon-only* defect line: a pedagogical example

In what follows, we shall illustrate the procedure described in Section 2 by working out the scattering of electrons from a *pentagon-only* defect line in the context of the first neighbor tight-binding model of graphene (see Fig. 3). As this system is invariant under translations along the defect line, Bloch's theorem allows the Fourier transformation along that direction. Therefore, the 2D graphene layer can be transformed into an effective 1D chain (see Fig. 4). This effective 1D chain depends on the quantum number k_x , the wave-number along \mathbf{u}_1 direction. Based on this 1D effective description, we can straightforwardly employ the procedure described in Section 2.

3.1. Formulating the problem

Let us assume we have the following system: a defect line of the type represented in Fig. 3, in an otherwise perfect graphene lattice.

As we can see by inspection of Fig. 3, the lattice vectors \mathbf{u}_1 and \mathbf{u}_2 , in cartesian coordinates, read

$$\mathbf{u}_1 = a(1, 0), \quad (15a)$$

$$\mathbf{u}_2 = a\left(-\frac{1}{2}, \frac{\sqrt{3}}{2}\right), \quad (15b)$$

where a stands for the lattice parameter.

Using this coordinate system, we can write the first neighbor tight-binding Hamiltonian of the system sketched in Fig. 3 as $\hat{H} = \hat{H}^U + \hat{H}^D + \hat{H}^L$, where \hat{H}^U (\hat{H}^L) stands for the Hamiltonian above (below) the defect line, while the remaining term, \hat{H}^D , describes the defect line itself. In second quantization the explicit forms of \hat{H}^U and \hat{H}^L read

$$\begin{aligned} \hat{H}^{U(L)} = & -t \sum_m \sum_n \left\{ \left[\hat{b}^\dagger(m, n) + \hat{b}^\dagger(m, n-1) \right. \right. \\ & \left. \left. + \hat{b}^\dagger(m-1, n-1) \right] \hat{a}(m, n) + h.c. \right\}, \end{aligned} \quad (16)$$

where for H^U (H^L), $n \geq 1$ ($n \leq -1$). Moreover, H^D reads

$$\hat{H}^D = -t \sum_m \left\{ \left[\xi \hat{d}^\dagger(m+1) + \hat{a}^\dagger(m, 0) + \hat{b}^\dagger(m, 0) \right] \hat{d}(m) + h.c. \right\}, \quad (17)$$

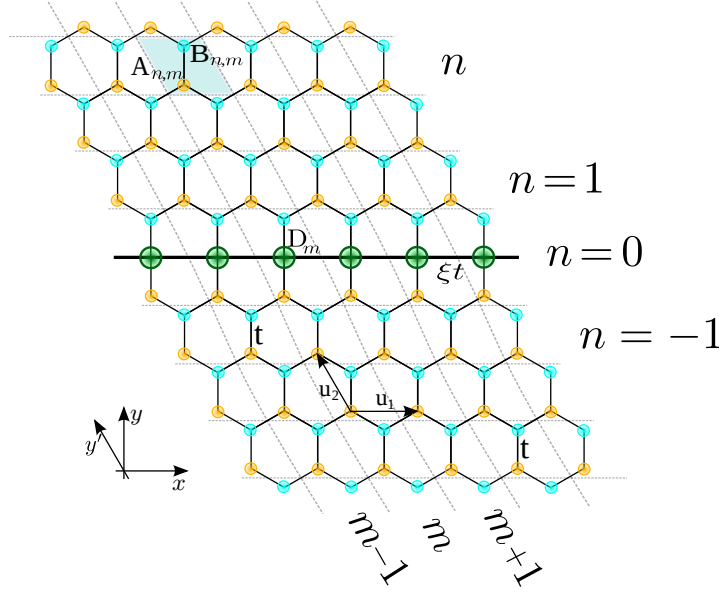


Figure 3. (Color online) Graphene's honeycomb lattice with a zigzag oriented linear defect, which we dub *pentagon-only* defect line. In the bulk the hopping is t , while between atoms of the defect it is ξt . The lattice vectors are denoted by $\mathbf{u}_1 = a(1, 0)$ and $\mathbf{u}_2 = (-1, \sqrt{3})a/2$, where a stands for the lattice parameter.

where t is the usual hopping amplitude of pristine graphene, while ξt is the hopping amplitude between the D_m atoms of the defect line, as represented in Fig. 3.

As was referred in the beginning of this section, this system is invariant under translations $\mathbf{r} = m\mathbf{u}_1$ (where m is an integer). Thus, we can make use of Bloch's theorem and Fourier transform the Hamiltonian along \mathbf{u}_1 . This diagonalizes the problem relatively to the variable m , introducing a new quantum number, k_x . Consequently, the resulting Hamiltonian turns out to be equivalent to the Hamiltonian of a one-dimensional chain with two atoms per unit cell and a localized defect at its center (see Fig. 4).

The Hamiltonian of the effective one-dimensional chain, can be written as $\hat{H}(k_x) = \hat{H}^U(k_x) + \hat{H}^D(k_x) + \hat{H}^L(k_x)$. Its three terms read

$$\hat{H}^{U(L)}(k_x) = - \sum_n \left\{ \left[t' \hat{b}^\dagger(k_x, n-1) + t \hat{b}^\dagger(k_x, n) \right] \hat{a}(k_x, n) + h.c. \right\}, \quad (18a)$$

$$\begin{aligned} \hat{H}^D(k_x) = & - 2\xi t \cos(k_x a) \hat{d}^\dagger(k_x) \hat{d}(k_x) - \left[t \hat{a}^\dagger(k_x, 0) \hat{d}(k_x) \right. \\ & \left. + t \hat{b}^\dagger(k_x, 0) \hat{d}(k_x) + h.c. \right]. \end{aligned} \quad (18b)$$

This one-dimensional chain has alternating hopping amplitudes between the atoms, t and $t' = t(1 + e^{ik_x a})$. At the defect, there is a on-site energy term, $\tilde{\epsilon}(k_x) = -2\xi t \cos(k_x a)$, which depends on the value of the longitudinal momentum k_x .

The TB equations of such system are, as usually, obtained from Schrödinger's equation

$$\hat{H}(k_x) |\mu, k_x\rangle = \epsilon_{\mu, k_x} |\mu, k_x\rangle. \quad (19)$$

In Eq. (19) $\hat{H}(k_x)$ stands for the Hamiltonian of the effective one-dimensional chain,

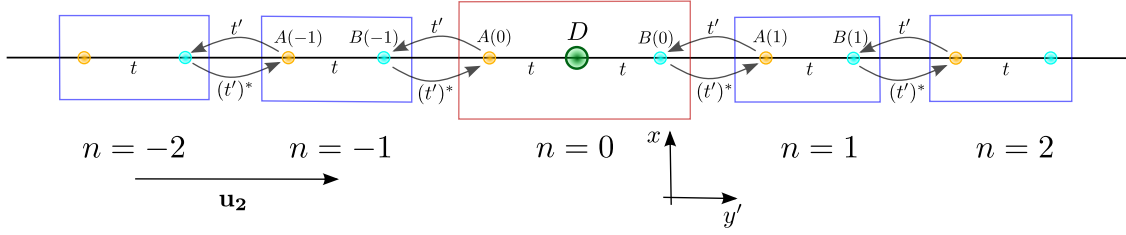


Figure 4. (Color online) Effective one-dimensional chain obtained after Fourier transforming the Hamiltonian of graphene with a *pentagon-only* defect line, along the \mathbf{u}_1 direction.

while the eigenstate $|\mu, k_x\rangle$ can be expressed as a linear combination of the site amplitudes along the one-dimensional chain

$$|\mu, k_x\rangle = \sum_{n=-\infty}^{+\infty} \left[A(k_x, n)|a; k_x, n\rangle + B(k_x, n)|b; k_x, n\rangle \right] + D(k_x)|d; k_x\rangle, \quad (20)$$

where the $|c; k_x, n\rangle = \hat{c}^\dagger(k_x, n)|0\rangle$ stands for the one-particle states at the atom $c = a, b, d$ of unit cell n of the one-dimensional chain.

3.2. Bulk properties

From what we have written above, it is simple to conclude that the TB equations in the bulk ($n \neq 0$) of the one-dimensional chain (see Fig. 4), read

$$\epsilon A(k_x, n) = -tB(k_x, n) - (t')^* B(k_x, n-1), \quad (21a)$$

$$\epsilon B(k_x, n) = -tA(k_x, n) - t' A(k_x, n+1). \quad (21b)$$

To recast these equations in the form of a transfer matrix relation, we solve Eq. (21b) for $A(k_x, n+1)$ and Eq. (21a) for $B(k_x, n)$

$$A(k_x, n+1) = -\frac{t}{t'} A(k_x, n) - \frac{\epsilon}{t'} B(k_x, n). \quad (22a)$$

$$B(k_x, n) = -\frac{\epsilon}{t} A(k_x, n) - \frac{(t')^*}{t} B(k_x, n-1), \quad (22b)$$

where we have used $t' = t(1 + e^{ik_x a})$. If now we write Eq. (22b) for $n+1$ and substitute Eq. (22a) in it, we obtain a recurrence relation between the amplitudes at unit cell $n+1$ and those at unit cell n

$$\mathbf{L}(n+1) = \mathbb{T}(\epsilon, k_x) \cdot \mathbf{L}(n), \quad (23)$$

where $\mathbf{L}(n) = [A(k_x, n), B(k_x, n)]^T$. The transfer matrix $\mathbb{T}(\epsilon, k_x)$ has the explicit form

$$\mathbb{T}(\epsilon, k_x) = -\frac{e^{-i\frac{k_x a}{2}}}{2 \cos\left(\frac{k_x a}{2}\right)} \begin{bmatrix} 1 & \frac{\epsilon}{t} \\ -\frac{\epsilon}{t} & 4 \cos^2\left(\frac{k_x a}{2}\right) - \frac{\epsilon^2}{t^2} \end{bmatrix}. \quad (24)$$

As said in Section 2, the eigenvalues and eigenvectors in the bulk are obtained from the diagonalization of the matrix $\mathbb{T}(\epsilon, k_x)$. In particular, eigenvalues of the transfer matrix which have unit modulus, $|\lambda|^2 = 1$, correspond to Bloch solutions propagating

along the one-dimensional chain (a band state); eigenvalues with a modulus that is different from one, $|\lambda|^2 \neq 1$, correspond to evanescent Bloch solutions. These evanescent solutions decrease with $n \rightarrow +\infty$ ($n \rightarrow -\infty$) when $|\lambda|^2 < 1$ ($|\lambda|^2 > 1$).

3.3. The defect

We now go on to write the TB equations at the defect (see Fig. 4), and work them out in such a way that we can write a boundary condition in the form given by Eq. (7).

The TB equations at the defect (see Fig. 4) are:

$$\epsilon A(k_x, 1) = -(t')^* B(k_x, 0) - t B(k_x, 1); \quad (25a)$$

$$\epsilon B(k_x, 0) = -t D(k_x) - t' A(k_x, 1); \quad (25b)$$

$$\epsilon D(k_x) = -t(A(k_x, 0) + B(k_x, 0)) - 2\xi t \cos(k_x a) D(k_x); \quad (25c)$$

$$\epsilon A(k_x, 0) = -(t')^* B(k_x, -1) - t D(k_x); \quad (25d)$$

$$\epsilon B(k_x, -1) = -t' A(k_x, 0) - t A(k_x, -1). \quad (25e)$$

As we have mentioned above, the aim is to obtain an equation relating the wave function at the two sides of the defect. With that in mind, we solve each equation in (25) for the rightmost amplitude appearing in it:

$$B(k_x, 1) = -\frac{\epsilon}{t} A(k_x, 1) - \frac{(t')^*}{t} B(k_x, 0), \quad (26a)$$

$$A(k_x, 1) = -\frac{\epsilon}{t'} B(k_x, 0) - \frac{t}{t'} D(k_x), \quad (26b)$$

$$B(k_x, 0) = -\frac{\epsilon + 2\xi t \cos(k_x a)}{t} D(k_x) - A(k_x, 0), \quad (26c)$$

$$D(k_x) = -\frac{\epsilon}{t} A(k_x, 0) - \frac{(t')^*}{t} B(k_x, -1), \quad (26d)$$

$$A(k_x, 0) = -\frac{\epsilon}{t'} B(k_x, -1) - \frac{t}{t'} A(k_x, -1). \quad (26e)$$

It is convenient to write the above set of equations in matrix form as

$$\begin{bmatrix} B(k_x, 1) \\ A(k_x, 1) \end{bmatrix} = - \begin{bmatrix} \frac{\epsilon}{t} & \frac{(t')^*}{t} \\ -1 & 0 \end{bmatrix} \begin{bmatrix} A(k_x, 1) \\ B(k_x, 0) \end{bmatrix}, \quad (27a)$$

$$\begin{bmatrix} A(k_x, 1) \\ B(k_x, 0) \end{bmatrix} = - \begin{bmatrix} \frac{\epsilon}{t'} & \frac{t}{t'} \\ -1 & 0 \end{bmatrix} \begin{bmatrix} B(k_x, 0) \\ D(k_x) \end{bmatrix}, \quad (27b)$$

$$\begin{bmatrix} B(k_x, 0) \\ D(k_x) \end{bmatrix} = - \begin{bmatrix} \frac{\epsilon}{t} + 2\xi \cos(k_x a) & 1 \\ -1 & 0 \end{bmatrix} \begin{bmatrix} D(k_x) \\ A(k_x, 0) \end{bmatrix}, \quad (27c)$$

$$\begin{bmatrix} D(k_x) \\ A(k_x, 0) \end{bmatrix} = - \begin{bmatrix} \frac{\epsilon}{t} & \frac{(t')^*}{t} \\ -1 & 0 \end{bmatrix} \begin{bmatrix} A(k_x, 0) \\ B(k_x, -1) \end{bmatrix}, \quad (27d)$$

$$\begin{bmatrix} A(k_x, 0) \\ B(k_x, -1) \end{bmatrix} = - \begin{bmatrix} \frac{\epsilon}{t'} & \frac{t}{t'} \\ -1 & 0 \end{bmatrix} \begin{bmatrix} B(k_x, -1) \\ A(k_x, -1) \end{bmatrix}. \quad (27e)$$

It is now straightforward to write the boundary condition connecting the two sides of the defect as

$$\mathbf{L}(1) = \mathbb{M}_{55} \cdot \mathbf{L}(-1), \quad (28)$$

where the matrix \mathbb{M}_{55} is a 2×2 matrix defined by

$$\mathbb{M}_{55} = R \cdot \mathbb{N}_1(\epsilon, k_x) \cdot \mathbb{N}_2(\epsilon, k_x) \cdot \mathbb{N}_3(\epsilon, k_x) \cdot \mathbb{N}_1(\epsilon, k_x) \cdot \mathbb{N}_2(\epsilon, k_x) \cdot R^T; \quad (29)$$

the matrix R is the σ_x Pauli matrix, used to interchange rows A and B . The matrices \mathbb{N}_1 , \mathbb{N}_2 , and \mathbb{N}_3 , after substituting $t' = t(1 + e^{ik_x a})$, read

$$\mathbb{N}_1(\epsilon, k_x) = - \begin{bmatrix} \frac{\epsilon}{t} & (1 + e^{-ik_x a}) \\ -1 & 0 \end{bmatrix}, \quad (30a)$$

$$\mathbb{N}_2(\epsilon, k_x) = - \frac{1}{1 + e^{ik_x a}} \begin{bmatrix} \frac{\epsilon}{t} & 1 \\ -(1 + e^{ik_x a}) & 0 \end{bmatrix}, \quad (30b)$$

$$\mathbb{N}_3(\epsilon, k_x) = - \begin{bmatrix} \frac{\epsilon + 2t\xi \cos(k_x a)}{t} & 1 \\ -1 & 0 \end{bmatrix}, \quad (30c)$$

From Eqs. (28)-(30) we conclude that matrix \mathbb{M}_{55} , and consequently the boundary condition imposed by the defect, depend both on the energy, ϵ , and on the longitudinal momentum, k_x .

3.4. Computing the scattering coefficients

Using the spectrum of modes allowed in the bulk of the one-dimensional chain [obtained from the transfer matrix $\mathbb{T}(\epsilon, k_x)$] and the boundary condition calculated above [see Eqs. (28)-(30)], we can now solve completely the scattering problem from a *pentagon-only* defect line.

We consider the scattering process in which we have an incoming mode from $n = -\infty$. In this situation, due to the presence of the defect at $n = 0$, there will be a reflected mode as well as a transmitted one. For now, let us suppose to be working at positive energy and around the $\nu = +1$ Dirac point [$\mathbf{K}_+ = (4\pi/3a, 0)$].

We choose to denote $|\Psi_{>}\rangle$ ($|\Psi_{<}\rangle$) as the positively (negatively) moving mode of the transfer matrix when we are around the \mathbf{K}_+ Dirac point. Furthermore, the eigenvalue associated with this mode is going to be denoted by $\lambda_{>}$ ($\lambda_{<}$). Therefore, we can write the wave function on each side of the defect as

$$|\Psi(n < 0)\rangle = \lambda_{>}^{n+1} |\Psi_{>}\rangle + \rho \lambda_{<}^{n+1} |\Psi_{<}\rangle, \quad (31a)$$

$$|\Psi(n > 0)\rangle = \tau \lambda_{>}^{n-1} |\Psi_{>}\rangle, \quad (31b)$$

where ρ and τ stand for the reflection and transmission scattering amplitudes, respectively.

The direction of propagation of each of the modes obtained by diagonalization of the transfer matrix, can be determined by calculating the corresponding current. It is shown in Appendix B that, for graphene, the current operator along the equivalent 1D-chain is $t\sigma_y/\hbar$; in Fig. B1 we plot the current associated with each one of the transfer

matrix's modes. For different choices of ϵ and k_x the incoming, reflected and transmitted modes must be chosen accordingly with the direction of propagation of the current.

In order to determine the scattering coefficients ρ and τ , following the procedure detailed in Section 2, we write Eq. (12) for this specific case, assuming an ordering of the modes as $\{|\Psi_{>}\rangle, |\Psi_{<}\rangle\}$; the resulting equation is

$$\begin{bmatrix} \tau \\ 0 \end{bmatrix}_{n=+1} = U^{-1} \mathbb{M}_{55} U \begin{bmatrix} 1 \\ \rho \end{bmatrix}_{n=-1}. \quad (32)$$

Solving the above linear system is trivial, resulting in

$$\rho = -\frac{(U^{-1} \mathbb{M}_{55} U)_{21}}{(U^{-1} \mathbb{M}_{55} U)_{22}}, \quad (33a)$$

$$\tau = \frac{\det(U^{-1} \mathbb{M}_{55} U)}{(U^{-1} \mathbb{M}_{55} U)_{22}}. \quad (33b)$$

3.5. The transmittance

In the context of graphene, we are mostly interested in the low-energy region of the spectrum, that is close to the Dirac points. Therefore, in what concerns the electronic transport, it is a natural choice to plot the transmittance, $T = |\tau|^2$ in terms of $\mathbf{q} = \mathbf{k} - \mathbf{K}_\nu$, where \mathbf{k} is measured from the center of the zone [see Fig. 5].

In the low-energy limit, the graphene quasi-particles impinging on the defect line are massless Dirac fermions with a wave-vector \mathbf{q} , which defines their propagation direction. Therefore, in this limit, it is intuitive to refer the transmittance to the angle θ that \mathbf{q} makes with the defect line. As a consequence, and despite the fact that we are not necessarily working at low energies, we will choose to express the transmittance (obtained from the TB model) in terms of ϵ and θ , instead of doing so in terms of ϵ and k_x . In Appendix D we show how starting from the expressions of $T(\epsilon, k_x)$ we can obtain the transmittance in terms of the energy and the angle θ , namely $T(\epsilon, \theta)$.

In Fig. B1 it can be seen that the two modes of the transfer matrix have opposite directions of propagation. The figure also shows that when the sign of the energy is changed, the direction of propagation of the modes is reversed. Suppose that for a given pair (ϵ, k_x) , the mode identified by θ (or $+q_y$) is the one with positive direction of propagation. Therefore, if we make the change $\epsilon \rightarrow -\epsilon$, then the mode propagating in the positive direction along the one-dimensional chain is now the one with $-\theta$ (or $-q_y$) [compare panels (b1) and (b2) of Fig. 5].

As a consequence, and for the sake of comparison between scattering processes occurring at positive energy and those happening at negative energy, we will plot the transmittance against the angle $\theta' = \theta$ when $\epsilon > 0$, and against the angle $\theta' = -\theta$ when $\epsilon < 0$.

In Fig. 6 we represent the transmittance $T = |\tau|^2$ as function of the angle θ (when $\epsilon > 0$ and $-\theta$ when $\epsilon < 0$), made between \mathbf{q} of the incoming particle and the barrier [see Fig. 5]. In the different panels of Fig. 6, we present the transmittance curves for several values of the energy. The curves in the latter figure refer to the Dirac point \mathbf{K}_+ . Those

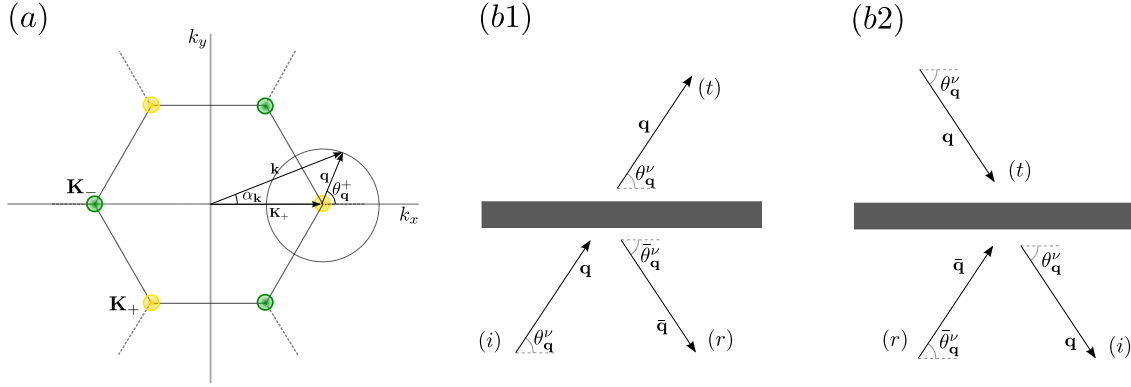


Figure 5. (Color online) (a) Pristine graphene FBZ where the incident wave vector, \mathbf{k} , is signaled, as well as the vector $\mathbf{q} = \mathbf{k} - \mathbf{K}_+$. (b) Schemes of the electron scattering across a defect line in 2D for low energy (wave vector around the Dirac cone) in two different cases: (b1) $\epsilon > 0$; (b2) $\epsilon < 0$. The labels (i) , (r) and (t) stand respectively for the incident, reflected and transmitted modes' wave-vectors.

referring to the Dirac point \mathbf{K}_- , are mirror symmetric to the former ones relatively to the axis $\theta = \pi/2$.

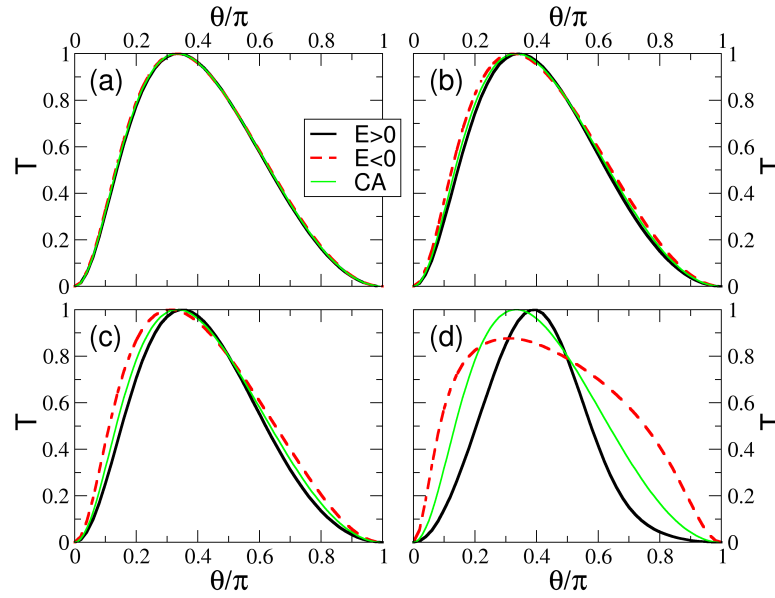


Figure 6. (Color online) Transmittance across the *pentagon-only* defect line as function of the incoming angle θ between \mathbf{q} (of the incoming particle) and the barrier. Remember that for negative energies, the transmittance is plotted against the angle $-\theta$. The hopping parameter at the defect, ξ , was fixed to $\xi = 1$ in this set of plots. The transmittance is plotted for several different modulus of the energy. These are: (a) $|\epsilon/t| = 0.01$; (b) $|\epsilon/t| = 0.05$; (c) $|\epsilon/t| = 0.1$; (d) $|\epsilon/t| = 0.5$. Positive energies are represented by the black full lines, while the negative ones are represented by the dashed red lines. The green full lines stand for the continuum low-energy result (that is energy-independent) as obtained in Ref. [16]. Only the curves associated with the Dirac point \mathbf{K}_+ are represented. Those for the Dirac point \mathbf{K}_- are obtained from the former by a reflection of these over the axis $\theta = \pi/2$.

As one can see in Fig. 6(a) and (b), the TB low-energy result (black full line and red dashed line) is in good accordance with that obtained in Ref. [16] using the continuum approximation (green full line).

The transmittance profile arising from the *pentagon-only* defect line is essentially controlled by the values of the hopping parameter ξ at the defect line [see Eqs. (33)]. Modifications of this hopping parameter, result in very different transmittance behaviors: the transmission amplitude for a given angle, θ , and a given energy, ϵ , is typically very different for distinct values of ξ ; in particular, the existence and position of an angle with perfect transmittance is strongly dependent on ξ .

Looking at Eq. (33b) one can easily conclude that it is its denominator that controls the transmittance, since, from Eq. (14) and Eq. (B.9), we have that $|\det(U^{-1}\mathbb{M}_{55}U)|^2 = 1$. Nevertheless, the analysis of the mathematical expression of $(U^{-1}\mathbb{M}_{55}U)_{22}$ gives us little physical intuition over the origin of an angle with perfect transmittance for a range of values of the hopping parameter ξ . Therefore, we will make use of the continuum low-energy description of this system, developed in Ref. [16], to investigate this feature of the transmittance.

As argued in Ref. [16], in the continuum low-energy limit, one can see the defect line as a strip of width W , where there is a general local potential, $\hat{V}(y) = V_s\mathbb{I} + V_x\sigma_x + V_y\sigma_y + V_z\sigma_z$. In the case of a *pentagon-only* defect line, one can show (see Appendix E) that the general local potential is of the form: $V_s \neq 0 \neq V_x$ and $V_y = 0 = V_z$. Inside the strip, the scalar potential term, V_s , changes the direction of propagation of the massless Dirac fermion, but keeps its spin aligned with its momentum (here and in the following paragraphs "spin" refers to the sub-lattice pseudo-spin degree of freedom). In contrast, the term V_x has the effect of not only changing the direction of propagation of the fermion inside the strip, but also of misaligning its spin and its momentum (see Appendix E). When $\epsilon, q_x \rightarrow 0$, the fermions inside the strip all propagate in the same direction, with the same misalignment between their spin and their momentum, and, therefore, share a common spin direction, at an angle $\alpha = \arccos(\xi/2)$ with the line defect.

At very low energies, fermions incident on the strip at an angle α have their spin already aligned with the spin direction inside the strip, and thus, their wave-functions outside and inside the strip can be matched without a reflected wave; the strip will be *invisible* to them and they will be totally transmitted across the defect line. Fermions at a different angle of incidence will have their spin outside and inside the strip misaligned, and thus will only be partly transmitted by the defect line. As a consequence, in the case of a *pentagon-only* defect line, the angle of perfect transmission (at very low energies) is exactly given by $\alpha = \arccos(\xi/2)$ [see Fig. 6(a)]. We see that this mechanism is entirely identical to that of perfect normal transmission across a barrier with a scalar potential [18]; the difference lies only with the presence of a V_x term, which induces misalignment between spin and momentum, and changes the direction along which spin alignment inside and outside the barrier occurs.

In the cases where $|\xi| > 2$, the wave-number associated with the fermions

propagating inside the strip, \tilde{q}_y , becomes imaginary: its wave-function is evanescent inside the strip. Moreover, α becomes imaginary and thus, the spin of the fermion has a non-zero z component. The fermions outside and inside the strip can never have their spins perfectly aligned. Their wave-functions cannot match without a reflected component, and there is no incident direction with perfect transmittance.

4. Scattering from a $zz(5757)$ and a $zz(558)$ defect line

In this section we consider two other types of extended defect lines, namely the $zz(5757)$ [16] and the $zz(558)$ defect lines [17, 8, 7] [see Fig. 7]. These defect lines are more realistic, albeit somewhat more complex to treat. We will see that both these defect lines give rise to a duplication of the unit cell. This originates a folding of the Brillouin zone, that brings to play two additional scattering modes. Despite the fact that at low-energies the latter happen to be evanescent modes, they must be considered in the computation of the scattering amplitudes.

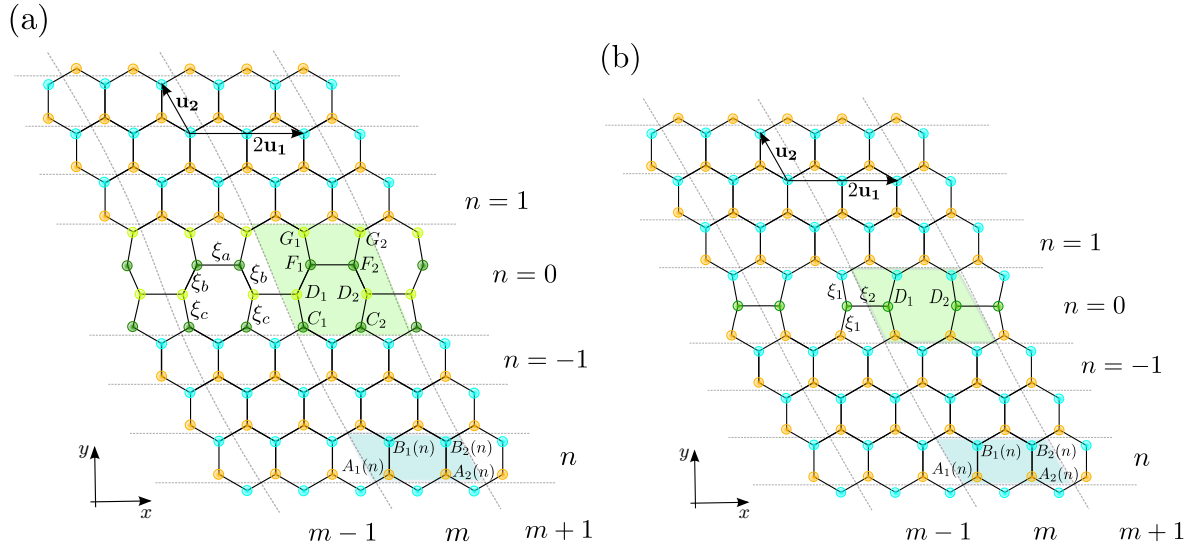


Figure 7. (Color online) Panel (a): Scheme of a $zz(5757)$ defect line. Panel (b): Scheme of a $zz(558)$ defect line.

The treatments of both the $zz(5757)$ and the $zz(558)$ defect lines are very similar to each other. The only difference between them is on the microscopic details of each defect line. As a consequence, and for the sake of definiteness, we shall first study electron scattering from a $zz(5757)$ defect line. We will employ again the procedure described in Section 2, which was previously applied to the study of the *pentagon-only* defect line (see Section 3). Afterwards, we will also compute the boundary condition arising from the $zz(558)$ defect line and we present the results for both the $zz(5757)$ and the $zz(558)$ cases.

4.1. Formulating the problem

Let us thus concentrate on the study of a graphene layer with a $zz(5757)$ defect line along the zigzag direction. As can be seen in Fig. 7(a), the $zz(5757)$ defect line has a periodicity twice as large as that of the *pentagon-only* defect line [see Fig. 3]. Therefore, its unit cell will necessarily be two times bigger in the defect direction, when compared with the unit cell of pristine graphene.

Then, the most natural choice for the lattice vectors is $2\mathbf{u}_1$ and \mathbf{u}_2 [where \mathbf{u}_1 and \mathbf{u}_2 were defined in Eq. (15)]. As a consequence the unit cell of bulk graphene will be twice as big in the \mathbf{u}_1 direction. Therefore, the First Brillouin Zone (FBZ) will be folded in comparison with the one of pristine graphene (see Fig. 8). The Dirac points will then be located at $\mathbf{K}_\nu = \nu\pi/(3a)(1, -\sqrt{3})$ (see Appendix D), where again, $\nu = \pm 1$ identifies the Dirac point.

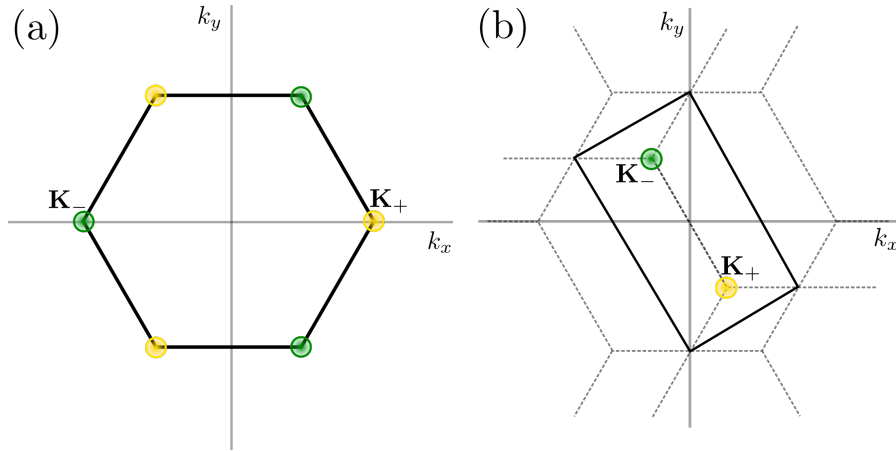


Figure 8. (Color online) Panel (a): Scheme of the FBZ of pristine graphene. Panel (b): Scheme of the FBZ of graphene with a doubled unit cell in \mathbf{u}_1 direction.

Let us now write the TB Hamiltonian of the graphene layer with a $zz(5757)$ defect line [see Fig. 7(a)]. As before, we can separate the Hamiltonian in three distinct parts: $\hat{H} = \hat{H}^U + \hat{H}^D + \hat{H}^L$, where \hat{H}^U (\hat{H}^L) stands for the Hamiltonian above (below) the defect line, while the remaining term, \hat{H}^D , describes the defect line itself. In second quantization the explicit forms of \hat{H}^U and \hat{H}^L read

$$H^{U(L)} = -t \sum_m \sum_n \left[\left(b_1^\dagger(m, n) + b_1^\dagger(m, n-1) + b_2^\dagger(m-1, n-1) \right) a_1(m, n) \right. \\ \left. + \left(b_2^\dagger(m, n) + b_1^\dagger(m, n-1) + b_2^\dagger(m, n-1) \right) a_2(m, n) + h.c. \right], \quad (34)$$

where for H^U (H^L) for $n \geq 1$ ($n \leq -1$).

Similarly, the term describing the TB Hamiltonian at the defect line reads

$$H^D = -t \sum_m \left[\left(\xi_c d_1^\dagger(m) + b_1^\dagger(m, -1) + b_2^\dagger(m-1, -1) \right) c_1(m) \right. \\ \left. + \left(\xi_c d_2^\dagger(m) + b_1^\dagger(m, -1) + b_2^\dagger(m, -1) \right) c_2(m) + \xi_a d_1^\dagger(m) d_2(m-1) \right]$$

$$\begin{aligned}
 & + \xi_a f_1^\dagger(m) f_2(m) + \xi_b d_1^\dagger(m) f_1(m) + \xi_b d_2^\dagger(m) f_2(m) + \left(\xi_c f_1^\dagger(m) \right. \\
 & + a_1^\dagger(m, 1) + a_2^\dagger(m, 1) \left. \right) g_1(m) + \left(\xi_c f_2^\dagger(m) + a_1^\dagger(m + 1, 1) \right. \\
 & \left. + a_2^\dagger(m, 1) \right) g_2(m) + h.c. \left. \right], \tag{35}
 \end{aligned}$$

where ξ_a , ξ_b and ξ_c stand for the renormalizations of the hopping amplitudes at the defect [see Fig. 7(a)].

Again the system is invariant under translations $\mathbf{r} = 2m\mathbf{u}_1$ (where m is an integer). Consequently, we can make use of Bloch theorem and Fourier transform the Hamiltonian along this direction, diagonalizing it with respect to the variable m . As expected, the resulting Hamiltonian turns out to be equivalent to the Hamiltonian describing a quasi-one-dimensional chain, with four atoms per unit cell and a defect at its center (see Fig. 9).

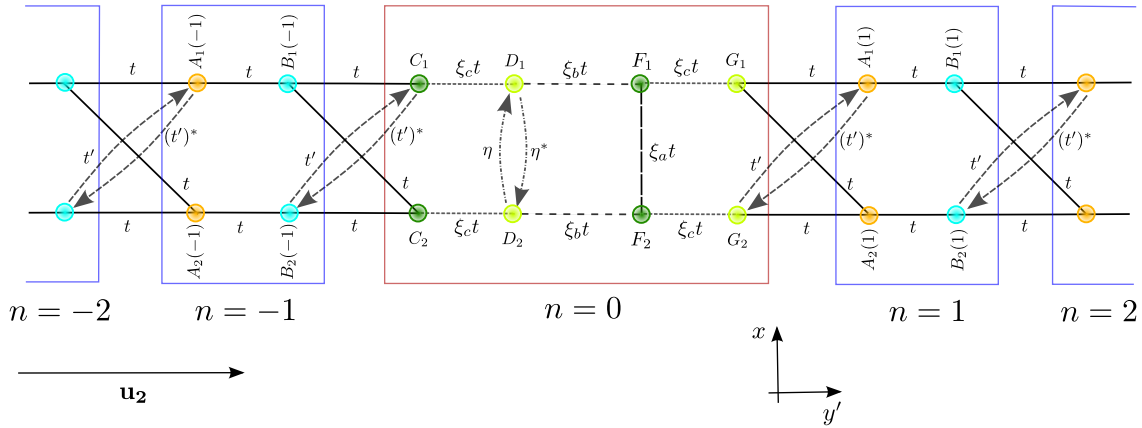


Figure 9. (Color online) Effective one-dimensional chain obtained after Fourier transforming the Hamiltonian of graphene with a $zz(5757)$ defect line. The hopping parameters t' and η , are short hands for $t' = te^{-i2k_x a}$ and for $\eta = t\xi_a e^{-i2k_x a}$. The parameters ξ_a , ξ_b and ξ_c stand for the hopping renormalizations appearing in Fig. 7(a).

Therefore, we can write the Hamiltonian of the effective one-dimensional chain as $H(k_x) = H^U(k_x) + H^D(k_x) + H^L(k_x)$. The part above and below the defect read

$$\begin{aligned}
 H^{U(L)}(k_x) = & -t \sum_n \left[\left(b_1^\dagger(k_x, n) + b_1^\dagger(k_x, n-1) + e^{i2k_x a} b_2^\dagger(k_x, n-1) \right) \right. \\
 & \times a_1(k_x, n) + \left(b_2^\dagger(k_x, n) + b_1^\dagger(k_x, n-1) + b_2^\dagger(k_x, n-1) \right) \\
 & \left. \times a_2(k_x, n) + h.c. \right], \tag{36}
 \end{aligned}$$

while the part corresponding to the defect reads

$$\begin{aligned}
 H^D(k_x) = & -t \left[\left(\xi_c d_1^\dagger(k_x) + b_1^\dagger(k_x, -1) + e^{i2k_x a} b_2^\dagger(k_x, -1) \right) c_1(k_x) + \left(\xi_c d_2^\dagger(k_x) \right. \right. \\
 & \left. \left. + b_1^\dagger(k_x, -1) + b_2^\dagger(k_x, -1) \right) c_2(k_x) + \xi_a e^{-i2k_x a} d_1^\dagger(k_x) d_2(k_x) \right]
 \end{aligned}$$

$$\begin{aligned}
& + \xi_a f_1^\dagger(k_x) f_2(k_x) + \xi_b d_1^\dagger(k_x) f_1(k_x) + \xi_b d_2^\dagger(k_x) f_2(k_x) + \left(\xi_c f_1^\dagger(k_x) \right. \\
& + a_1^\dagger(k_x, 1) + a_2^\dagger(k_x, 1) \Big) g_1(k_x) + \left(\xi_c f_2^\dagger(k_x) + e^{-i2k_x a} a_1^\dagger(k_x, 1) \right. \\
& \left. + a_2^\dagger(k_x, 1) \Big) g_2(k_x) + h.c. \right]. \tag{37}
\end{aligned}$$

As was stated in Section 3.1, the TB equations of this system are obtained from its Schrödinger equation, $\hat{H}(k_x)|\mu, k_x\rangle = \epsilon_{\mu, k_x}|\mu, k_x\rangle$. In this last equation, $\hat{H}(k_x)$ stands for the Hamiltonian of the effective one-dimensional chain given by Eqs. (36)-(37). At the same time, the eigenstate $|\mu, k_x\rangle$ can be expressed as a linear combination of the site amplitudes along the one-dimensional chain:

$$\begin{aligned}
|\mu, k_x\rangle &= \sum_{i=1}^2 \sum_{n \neq 0} \left[A_i(k_x, n) |a_i; k_x, n\rangle + B_i(k_x, n) |b_i; k_x, n\rangle \right] \\
&+ \sum_{i=1}^2 \left[C_i(k_x) |c_i; k_x\rangle + D_i(k_x) |d_i; k_x\rangle + F_i(k_x) |f_i; k_x\rangle \right. \\
&\left. + G_i(k_x) |g_i; k_x\rangle \right], \tag{38}
\end{aligned}$$

where the $|z_i; k_x, n\rangle = \hat{z}_i^\dagger(k_x, n)|0\rangle$ stand for the one-particle states at the atom Z_i of unit cell n of the one-dimensional chain [with $z = a, b$ on the bulk ($n \neq 0$) and $z = c, d, f, g$ at the defect ($n = 0$)].

4.2. Bulk properties

From the above discussion, we can readily write the TB equations in the bulk ($n \neq 0$) of the quasi-one-dimensional chain. They read

$$\epsilon A_1(k_x, n) = -tB_1(k_x, n) - tB_1(k_x, n-1) - te^{-i2k_x a} B_2(k_x, n-1), \tag{39a}$$

$$\epsilon B_1(k_x, n) = -tA_1(k_x, n) - tA_1(k_x, n+1) - tA_2(k_x, n+1), \tag{39b}$$

$$\epsilon A_2(k_x, n) = -tB_2(k_x, n) - tB_1(k_x, n-1) - tB_2(k_x, n-1), \tag{39c}$$

$$\epsilon B_2(k_x, n) = -tA_2(k_x, n) - te^{i2k_x a} A_1(k_x, n+1) - tA_2(k_x, n+1). \tag{39d}$$

As before, we can write a recurrence relation between the amplitudes of the unit cell located at position n and those of the unit cell located at position $n+1$. Following a procedure similar to that leading to Eqs. (23) and (24), one obtains

$$\mathbf{L}(n+1) = \mathbb{T}(\epsilon, k_x) \cdot \mathbf{L}(n), \tag{40}$$

where $\mathbf{L}(n) = [A_1(k_x, n), B_1(k_x, n), A_2(k_x, n), B_2(k_x, n)]^T$, and the transfer matrix, $\mathbb{T}(\epsilon, k_x)$, has the following form

$$\mathbb{T}(\epsilon, k_x) = -\frac{1}{1 - e^{i2k_x a}} \begin{bmatrix} -1 & 1 & -\epsilon & \epsilon \\ e^{i2k_x a} & -1 & \frac{\epsilon}{e^{-i2k_x a}} & -\epsilon \\ \epsilon & -\epsilon & w(\epsilon, k_x) & -w(\epsilon, -k_x) \\ \frac{-\epsilon}{e^{-i2k_x a}} & \epsilon & \frac{-w(\epsilon, -k_x)}{e^{-i2k_x a}} & w(\epsilon, k_x) \end{bmatrix}, \tag{41}$$

where $w(\epsilon, k_x) = -1 + e^{i2k_x a} + \epsilon^2$.

If we take into account the nature of the folding of the FBZ, we can make a basis change that will turn the transfer matrix $\mathbb{T}(\epsilon, k_x)$ into a block diagonal matrix (see Appendix C). Such a basis change groups the modes in two distinct pairs, uncoupling the bulk descriptions of each one of these pairs. We dub the modes of one of those pairs as the $+$ modes, while the modes of the other are going to be called $-$ modes. Each one of these pairs of modes is associated with a pair of energy bands present in the folded FBZ. Note, for instance, that when we position ourselves near the Dirac points, $\mathbf{K}_\nu = \nu\pi/3(1/a, -\sqrt{3}/a)$, the $+$ modes turn out to be high in energy ($\epsilon_+ \approx 2t$), while the $-$ modes are low in energy ($\epsilon_- \approx 0$) [19].

The latter basis change reads

$$\bar{\mathbf{L}}(n) = \Lambda(k_x) \cdot \mathbf{L}(n), \quad (42)$$

where $\bar{\mathbf{L}}(n) = [A_+(k_x, n), B_+(k_x, n), A_-(k_x, n), B_-(k_x, n)]^T$, while the matrix $\Lambda(k_x)$, reads (see Appendix C)

$$\Lambda(k_x) = \frac{1}{\sqrt{2}} \begin{bmatrix} 1 & 0 & e^{-ik_x a} & 0 \\ 0 & 1 & 0 & e^{-ik_x a} \\ 1 & 0 & -e^{-ik_x a} & 0 \\ 0 & 1 & 0 & -e^{-ik_x a} \end{bmatrix}. \quad (43)$$

Applying this transformation to the transfer matrix (41) we obtain $\bar{\mathbb{T}}(\epsilon, k_x) = \Lambda(k_x)\mathbb{T}(\epsilon, k_x)\Lambda^{-1}(k_x)$, where

$$\bar{\mathbb{T}}(\epsilon, k_x) = \begin{bmatrix} \mathbb{T}_+(\epsilon, k_x) & 0 \\ 0 & \mathbb{T}_-(\epsilon, k_x) \end{bmatrix}. \quad (44)$$

is block diagonal. In the above expression, \mathbb{T}_+ and \mathbb{T}_- are 2×2 transfer matrices associated with the $+$ and the $-$ modes, respectively. These matrices are given by:

$$\mathbb{T}_+(\epsilon, k_x) = -\frac{e^{-i\frac{k_x a}{2}}}{2 \cos(\frac{k_x a}{2})} \begin{bmatrix} 1 & \frac{\epsilon}{t} \\ -\frac{\epsilon}{t} & 4 \cos^2(\frac{k_x a}{2}) - \frac{\epsilon^2}{t^2} \end{bmatrix}; \quad (45a)$$

$$\mathbb{T}_-(\epsilon, k_x) = \frac{e^{-i\frac{k_x a}{2}}}{2i \sin(\frac{k_x a}{2})} \begin{bmatrix} 1 & \frac{\epsilon}{t} \\ -\frac{\epsilon}{t} & 4 \sin^2(\frac{k_x a}{2}) - \frac{\epsilon^2}{t^2} \end{bmatrix}. \quad (45b)$$

Again, as was said in Section 2, the eigenvalues and eigenvectors of the transfer matrix $\bar{\mathbb{T}}$ give the Bloch solutions of the problem. Eigenvalues with unit modulus, $|\lambda|^2 = 1$, correspond to Bloch solutions propagating along the one-dimensional chain (a band state), while eigenvalues with non-unit modulus, $|\lambda|^2 \neq 1$, correspond to evanescent Bloch solutions [decreasing with $n \rightarrow +\infty$ ($n \rightarrow -\infty$) when $|\lambda|^2 < 1$ ($|\lambda|^2 > 1$)].

Moreover, in the basis that uncouples $+$ and $-$ modes the matrices \mathbb{T}_+ and \mathbb{T}_- give the Bloch solutions associated with each one of the $+$ and $-$ energy sectors. Again, these can be either propagating or evanescent depending on the energy ϵ and momentum k_x . Of relevance is the case where the scattering process occurs at a sufficiently small energy ($\epsilon \lesssim 2t$) so that we are sufficiently near the Dirac points. In this case, the $+$ modes turn out to be evanescent while the $-$ ones are still propagating. When we are

at very low-energies, $\epsilon \approx 0$, the transfer matrices associated with each pair of modes read

$$\mathbb{T}_+\left(0, \nu \frac{\pi}{3a}\right) = -e^{-i\nu \frac{\pi}{6}} \begin{bmatrix} \frac{1}{\sqrt{3}} & 0 \\ 0 & \sqrt{3} \end{bmatrix}, \quad (46a)$$

$$\mathbb{T}_-\left(0, \nu \frac{\pi}{3a}\right) = e^{-i\nu \frac{2\pi}{3}} \begin{bmatrix} 1 & 0 \\ 0 & 1 \end{bmatrix}. \quad (46b)$$

Thus, we can conclude that the $+$ modes are evanescent either decreasing or increasing exponentially as $e^{-n \log \sqrt{3}}$ or as $e^{n \log \sqrt{3}}$ with increasing n . At the same time the $-$ modes are propagating.

4.3. The $zz(5757)$ defect

It is important to note that the conclusions of Section 4.2 apply not only to the case of the $zz(5757)$ defect line, but also to the $zz(558)$ defect line. In fact, the reasoning pursued in Section 4.2 describes the bulk of systems whose unit cell's size in the direction of \mathbf{u}_1 is twice that of pristine graphene. As we can readily conclude from Fig. 7, both the $zz(5757)$ defect line and the $zz(558)$ one impose the same duplication of the unit cell along the zigzag direction. As a consequence, the bulk problem of these two systems is described by the same transfer matrix relations, Eqs. (41)-(45).

As previously noted, what distinguishes electron scattering in the $zz(5757)$ and in the $zz(558)$ defect lines are the microscopic details of each one of these defects. Next we will show how to compute the boundary condition relation for each one of these two defect lines.

Let us start by the case of the $zz(5757)$ defect. From Eqs. (37) and (38) we write the TB equations at the $zz(5757)$ defect. They read

$$-\frac{\epsilon}{t} \mathbf{A}(1) = W_A^\dagger \mathbf{G}(0) + \mathbf{B}(1), \quad (47a)$$

$$-\frac{\epsilon}{t} \mathbf{G}(0) = \xi_c \mathbf{F}(0) + W_A \mathbf{A}(1), \quad (47b)$$

$$-\frac{\epsilon}{t} \mathbf{F}(0) = \xi_b \mathbf{D}(0) + \xi_c \mathbf{G}(0) + \xi_a \sigma_x \mathbf{F}(0), \quad (47c)$$

$$-\frac{\epsilon}{t} \mathbf{D}(0) = \xi_c \mathbf{C}(0) + \xi_b \mathbf{F}(0) + \xi_a \sigma'_x \mathbf{D}(0), \quad (47d)$$

$$-\frac{\epsilon}{t} \mathbf{C}(0) = W_A^\dagger \mathbf{B}(-1) + \xi_c \mathbf{D}(0), \quad (47e)$$

$$-\frac{\epsilon}{t} \mathbf{B}(-1) = \mathbf{A}(-1) + W_A \mathbf{C}(0), \quad (47f)$$

where $\mathbf{Z}(n) = [Z_1(n), Z_2(n)]^T$, for $Z = A, B, C, D, F, G$. The matrices W_A , σ_x and σ'_x appearing in Eqs. (47), are given by

$$W_A = \begin{bmatrix} 1 & 1 \\ e^{2ik_x a} & 1 \end{bmatrix}, \quad (48a)$$

$$\sigma_x = \begin{bmatrix} 0 & 1 \\ 1 & 0 \end{bmatrix}, \quad (48b)$$

$$\sigma'_x = \begin{bmatrix} 0 & e^{-2ik_x a} \\ e^{2ik_x a} & 0 \end{bmatrix}. \quad (48c)$$

In close analogy with what was done for the case of the *pentagon-only* defect line, and after some elementary algebraic manipulations, we can rewrite the above 2×2 matrix equations in a more compact form:

$$\begin{bmatrix} \mathbf{B}(1) \\ \mathbf{A}(1) \end{bmatrix} = - \begin{bmatrix} \frac{\epsilon}{t} \mathbb{I}_2 & (W_A)^\dagger \\ -\mathbb{I}_2 & 0 \end{bmatrix} \begin{bmatrix} \mathbf{A}(1) \\ \mathbf{G}(0) \end{bmatrix}, \quad (49a)$$

$$\begin{bmatrix} \mathbf{A}(1) \\ \mathbf{G}(0) \end{bmatrix} = - \begin{bmatrix} \frac{\epsilon}{t} (W_A)^{-1} & \xi_c (W_A)^{-1} \\ -\mathbb{I}_2 & 0 \end{bmatrix} \begin{bmatrix} \mathbf{G}(0) \\ \mathbf{F}(0) \end{bmatrix}, \quad (49b)$$

$$\begin{bmatrix} \mathbf{G}(0) \\ \mathbf{F}(0) \end{bmatrix} = - \begin{bmatrix} \frac{1}{\xi_c} \left(\frac{\epsilon}{t} \mathbb{I}_2 + \xi_a \sigma_x \right) & \frac{\xi_b}{\xi_c} \mathbb{I}_2 \\ -\mathbb{I}_2 & 0 \end{bmatrix} \begin{bmatrix} \mathbf{F}(0) \\ \mathbf{D}(0) \end{bmatrix}, \quad (49c)$$

$$\begin{bmatrix} \mathbf{F}(0) \\ \mathbf{D}(0) \end{bmatrix} = - \begin{bmatrix} \frac{1}{\xi_b} \left(\frac{\epsilon}{t} \mathbb{I}_2 + \xi_a \sigma'_x \right) & \frac{\xi_c}{\xi_b} \mathbb{I}_2 \\ -\mathbb{I}_2 & 0 \end{bmatrix} \begin{bmatrix} \mathbf{G}(0) \\ \mathbf{C}(0) \end{bmatrix}, \quad (49d)$$

$$\begin{bmatrix} \mathbf{D}(0) \\ \mathbf{C}(0) \end{bmatrix} = - \begin{bmatrix} \frac{\epsilon}{t \xi_c} \mathbb{I}_2 & \frac{1}{\xi_c} (W_A)^\dagger \\ -\mathbb{I}_2 & 0 \end{bmatrix} \begin{bmatrix} \mathbf{C}(0) \\ \mathbf{B}(-1) \end{bmatrix}, \quad (49e)$$

$$\begin{bmatrix} \mathbf{C}(0) \\ \mathbf{B}(-1) \end{bmatrix} = - \begin{bmatrix} \frac{\epsilon}{t} (W_A)^{-1} & (W_A)^{-1} \\ -\mathbb{I}_2 & 0 \end{bmatrix} \begin{bmatrix} \mathbf{B}(-1) \\ \mathbf{A}(-1) \end{bmatrix}, \quad (49f)$$

where \mathbb{I}_2 stands for the 2×2 unit matrix. Note that Eqs. (49) are now 4×4 matrix equations. In what follows we are going to denote the matrices in Eqs. (49a), (49b), (49c), (49d), (49e) and (49f) by $\mathbb{P}_1(\epsilon, k_x)$, $\mathbb{P}_2(\epsilon, k_x)$, $\mathbb{P}_3(\epsilon, k_x)$, $\mathbb{P}_4(\epsilon, k_x)$, $\mathbb{P}_5(\epsilon, k_x)$ and $\mathbb{P}_6(\epsilon, k_x)$, respectively.

The boundary condition matrix equation relating the vectors

$$\mathbf{L}(1) = [A_1(k_x, 1), B_1(k_x, 1), A_2(k_x, 1), B_2(k_x, 1)]^T \quad (50)$$

and

$$\mathbf{L}(-1) = [A_1(k_x, -1), B_1(k_x, -1), A_2(k_x, -1), B_2(k_x, -1)]^T, \quad (51)$$

becomes

$$\mathbf{L}(1) = \mathbb{M}_{5757} \cdot \mathbf{L}(-1). \quad (52)$$

In the above equation, the boundary condition matrix, \mathbb{M}_{5757} , is a 4×4 matrix (in contrast with the case of the *pentagon-only* defect line) and is given by

$$\mathbb{M}_{5757} = R \cdot \mathbb{P}_1 \cdot \mathbb{P}_2 \cdot \mathbb{P}_3 \cdot \mathbb{P}_4 \cdot \mathbb{P}_5 \cdot \mathbb{P}_6 \cdot R^T, \quad (53)$$

where, for the sake of simplicity of notation, we have omitted the dependence of the matrices \mathbb{P}_i on ϵ and on k_x ; the matrix R in Eq. (52) makes a basis change from $\{B_1, B_2, A_1, A_2\}$ to $\{A_1, B_1, A_2, B_2\}$, and is defined by

$$R = \begin{bmatrix} 0 & 0 & 1 & 0 \\ 1 & 0 & 0 & 0 \\ 0 & 0 & 0 & 1 \\ 0 & 1 & 0 & 0 \end{bmatrix}. \quad (54)$$

It is worth commenting that, if we change to the basis that uncouples the + and - energy sectors, $\overline{\mathbb{M}}_{5757}(\epsilon, k_x) = \Lambda \mathbb{M}_{5757}(\epsilon, k_x) \Lambda^{-1}$ [where matrix Λ is defined in Eq. (43)], we readily conclude that the boundary condition matrix mixes + and - modes on opposite sides of the defect.

4.4. The $zz(558)$ defect

We can employ an entirely analogous procedure to the $zz(558)$ defect. As before, we can write the Hamiltonian describing such a system, and from it we write the TB equations at the $zz(558)$ defect [see Fig. 7(b)]. These read

$$-\frac{\epsilon}{t} \mathbf{A}(1) = W_A^\dagger \mathbf{B}(0) + \mathbf{B}(1), \quad (55a)$$

$$-\frac{\epsilon}{t} \mathbf{B}(0) = \xi_1 \mathbf{D}(0) + W_A \mathbf{A}(1), \quad (55b)$$

$$-\frac{\epsilon}{t} \mathbf{D}(0) = \xi_1 \mathbf{B}(0) + \xi_2 \sigma'_x \mathbf{D}(0) + \xi_1 \mathbf{A}(0), \quad (55c)$$

$$-\frac{\epsilon}{t} \mathbf{A}(0) = \xi_1 \mathbf{D}(0) + W_A^\dagger \mathbf{B}(-1), \quad (55d)$$

$$-\frac{\epsilon}{t} \mathbf{B}(-1) = \mathbf{A}(-1) + W_A \mathbf{A}(0), \quad (55e)$$

where, once more we use the notation $\mathbf{Z}(n) = [Z_1(n), Z_2(n)]^T$, for $Z = A, B, D$.

As before, we can easily rewrite the above 2×2 matrix equations in a more compact form

$$\begin{bmatrix} \mathbf{B}(1) \\ \mathbf{A}(1) \end{bmatrix} = - \begin{bmatrix} \frac{\epsilon}{t} \mathbb{I}_2 & (W_A)^\dagger \\ -\mathbb{I}_2 & 0 \end{bmatrix} \begin{bmatrix} \mathbf{A}(1) \\ \mathbf{B}(0) \end{bmatrix}, \quad (56a)$$

$$\begin{bmatrix} \mathbf{A}(1) \\ \mathbf{B}(0) \end{bmatrix} = - \begin{bmatrix} \frac{\epsilon}{t} (W_A)^{-1} & \xi_1 (W_A)^{-1} \\ -\mathbb{I}_2 & 0 \end{bmatrix} \begin{bmatrix} \mathbf{B}(0) \\ \mathbf{D}(0) \end{bmatrix}, \quad (56b)$$

$$\begin{bmatrix} \mathbf{B}(0) \\ \mathbf{D}(0) \end{bmatrix} = - \begin{bmatrix} \frac{1}{\xi_1} \left(\frac{\epsilon}{t} \mathbb{I}_2 + \xi_2 \sigma'_x \right) & \mathbb{I}_2 \\ -\mathbb{I}_2 & 0 \end{bmatrix} \begin{bmatrix} \mathbf{D}(0) \\ \mathbf{A}(0) \end{bmatrix}, \quad (56c)$$

$$\begin{bmatrix} \mathbf{D}(0) \\ \mathbf{A}(0) \end{bmatrix} = - \begin{bmatrix} \frac{\epsilon}{t \xi_1} \mathbb{I}_2 & \frac{1}{\xi_1} (W_A)^\dagger \\ -\mathbb{I}_2 & 0 \end{bmatrix} \begin{bmatrix} \mathbf{A}(0) \\ \mathbf{B}(-1) \end{bmatrix}, \quad (56d)$$

$$\begin{bmatrix} \mathbf{A}(0) \\ \mathbf{B}(-1) \end{bmatrix} = - \begin{bmatrix} \frac{\epsilon}{t} (W_A)^{-1} & (W_A)^{-1} \\ -\mathbb{I}_2 & 0 \end{bmatrix} \begin{bmatrix} \mathbf{B}(-1) \\ \mathbf{A}(-1) \end{bmatrix}. \quad (56e)$$

The 4×4 matrices appearing on the right hand side of Eqs. (56a), (56b), (56c), (56d) and (56e) will be denoted by $\mathbb{Q}_1(\epsilon, k_x)$, $\mathbb{Q}_2(\epsilon, k_x)$, $\mathbb{Q}_3(\epsilon, k_x)$, $\mathbb{Q}_4(\epsilon, k_x)$ and $\mathbb{Q}_5(\epsilon, k_x)$, respectively.

The boundary condition matrix equation relating $\mathbf{L}(1)$ and $\mathbf{L}(-1)$ is of the same form as in Eq. (52)

$$\mathbf{L}(1) = \mathbb{M}_{558} \cdot \mathbf{L}(-1), \quad (57)$$

where, the boundary condition matrix, \mathbb{M}_{558} , is a 4×4 matrix now given by

$$\mathbb{M}_{558} = R \cdot \mathbb{Q}_1 \cdot \mathbb{Q}_2 \cdot \mathbb{Q}_3 \cdot \mathbb{Q}_4 \cdot \mathbb{Q}_5 \cdot R^T, \quad (58)$$

where again, for the sake of simplicity of notation, we have omitted the dependence of the matrices \mathbb{Q}_i on ϵ and on k_x .

Once again, in the basis that uncouples the $+$ and the $-$ modes, $\overline{\mathbb{M}}_{558}(\epsilon, k_x) = \Lambda \mathbb{M}_{558} \Lambda^{-1}$ [where matrix Λ is defined in Eq. (43)], one readily sees that the boundary condition matrix also mixes the modes of the $+$ and the $-$ energy sectors of opposite sides of the defect.

4.5. Computing the scattering coefficients

The scattering problem from the $zz(5757)$ [and the $zz(558)$] defect line can now be solved completely using the boundary condition at the defect, Eqs. (53) [Eq. (58)], and the modes allowed in the bulk [obtained from the transfer matrix, Eq. (44)-(45)].

Let us suppose that we are working at positive energy and around the $\nu = +1$ Dirac point [$\mathbf{K}_+ = \pi/3(1/a, -\sqrt{3}/a)$]. Moreover, we suppose that the energy is small, so that the $+$ modes are evanescent. We then consider the scattering process in which we have one incoming mode from $n = -\infty$ associated with the $-$ energy sector. Due to the presence of the defect at $n = 0$, there will be a reflected as well as a transmitted mode. Besides, in accordance with what was said above, there will be two evanescent modes associated with the $+$ energy sector.

We choose to denote $|\Psi_{>}^{(-)}\rangle$ ($|\Psi_{<}^{(-)}\rangle$) as the right (left) moving mode associated with the $-$ energy sector of the transfer matrix [see Eqs. (41)-(45)] when we are both at $\epsilon > 0$ and around the \mathbf{K}_+ Dirac point; the corresponding eigenvalues are denoted by $\lambda_{>}^{(-)}$ ($\lambda_{<}^{(-)}$). Similarly, we denote by $|\Psi_{>}^{(+)}\rangle$ ($|\Psi_{<}^{(+)}\rangle$) the $+$ energy sector's transfer matrix mode [see Eq. (41)-(45)], which decreases (increases) in the direction of \mathbf{u}_2 . This mode's corresponding eigenvalue is going to be denoted by $\lambda_{>}^{(+)}$ ($\lambda_{<}^{(+)}$.) We can thus write the wave function on each side of the defect as

$$\begin{aligned} \mathbf{L}(n < 0) &= (\lambda_{>}^{(-)})^{n+1} |\Psi_{>}^{(-)}\rangle + \rho_- (\lambda_{<}^{(-)})^{n+1} |\Psi_{<}^{(-)}\rangle \\ &\quad + \rho_+ (\lambda_{<}^{(+)})^{n+1} |\Psi_{<}^{(+)}\rangle, \end{aligned} \quad (59a)$$

$$\mathbf{L}(n > 0) = \tau_- (\lambda_{>}^{(-)})^{n-1} |\Psi_{>}^{(-)}\rangle + \tau_+ (\lambda_{>}^{(+)})^{n-1} |\Psi_{>}^{(+)}\rangle, \quad (59b)$$

where ρ_- and τ_- (ρ_+ and τ_+) are the reflection and transmission scattering amplitudes of the $-$ ($+$) modes, respectively.

As before, for different choices of ϵ and k_x the incoming, reflected, transmitted and evanescent modes must be chosen accordingly with the direction of propagation and/or direction of increase of the eigenmodes of the transfer matrix (see Fig. B2).

In order to determine the scattering coefficients ρ_{\pm} and τ_{\pm} , and in accordance with Section 2, we just need to substitute Eqs. (59) in the boundary condition expression arising from the $zz(5757)$ [$zz(558)$] defect, Eq. (52) [Eq. (57)]. to obtain the equivalent

of Eq. (12) for these cases,

$$\begin{bmatrix} \tau_+ \\ 0 \\ \tau_- \\ 0 \end{bmatrix}_{n=+1} = U^{-1} \mathbb{M} U \begin{bmatrix} 0 \\ \rho_+ \\ 1 \\ \rho_- \end{bmatrix}_{n=-1}, \quad (60)$$

where we have omitted the subscripts identifying the boundary condition matrix [either \mathbb{M}_{5757} for the $zz(5757)$ defect, or \mathbb{M}_{558} for the $zz(558)$]. In the above equation, the matrix U is the matrix mediating the basis transformation from the basis $\{A_+, B_+, A_-, B_-\}$ to the proper basis of the transfer matrix. As stated in Section 2, each column of U is one of the eigenmodes of the transfer matrix $U = [|\Psi_{>}^{(+)}\rangle, |\Psi_{<}^{(+)}\rangle, |\Psi_{>}^{(-)}\rangle, |\Psi_{<}^{(-)}\rangle]$, written in the $\{A_+, B_+, A_-, B_-\}$ basis.

Solving the above linear system of four equations can be readily accomplished with a computer algebra system. Its solution determines completely the scattering amplitudes of the problem.

4.6. The transmittance

As before, we are interested in computing the transmittance for relatively low-energies, which is equivalent to say that we want to compute the transmittance around the Dirac points. Consequently, the $+$ modes will be evanescent while the $-$ modes will be propagating. Therefore the transmittance is going to be given by $T = |\tau_-|^2$.

Similarly to what was done for the transmittance in the *pentagon-only* defect case, here, and for the sake of comparison between scattering processes occurring at positive and negative energy, we will plot the transmittance against $\theta' = \theta$ when $\epsilon > 0$, plotting it against $\theta' = -\theta$ when $\epsilon < 0$.

In Fig. 10 we represent the transmittance $T = |\tau_-|^2$ [associated both with the $zz(5757)$ and the $zz(558)$ defect lines] as function of the angle θ (when $\epsilon > 0$ and $-\theta$ when $\epsilon < 0$), made between \mathbf{q} and the defect line. In the several panels of Fig. 10, we present the transmittance curves for different values of the energy [the ones referring to the $zz(5757)$ defect are those in panels (a), while the ones referring to the $zz(558)$ defect are those in panels (b)]. The curves in the Fig. 10 refer to the Dirac point \mathbf{K}_+ . Those referring to the Dirac point \mathbf{K}_- , are mirror symmetric relatively to the line $\theta = \pi/2$ to the ones presented in the figure. In order to obtain the transmittance curves of Fig. 10, all hopping renormalizations were set equal to one in both defects: $\xi_a = \xi_b = \xi_c = 1$ and $\xi_1 = \xi_2 = 1$.

Again, the transmittance profile arising from each of these defect lines is controlled by the values of the hopping parameters at the defect line: ξ_1 and ξ_2 in the case of $zz(558)$ defect line; ξ_a , ξ_b and ξ_c in the case of the $zz(5757)$ defect line. Modifications of these parameters result in very different transmittance behaviors.

Here as in the *pentagon-only* defect case, the analysis of the TB expressions giving the transmission amplitude, Eq. (60), is of little help concerning physical intuition over the presence of perfect transmittance angles for certain ranges of values for the hopping

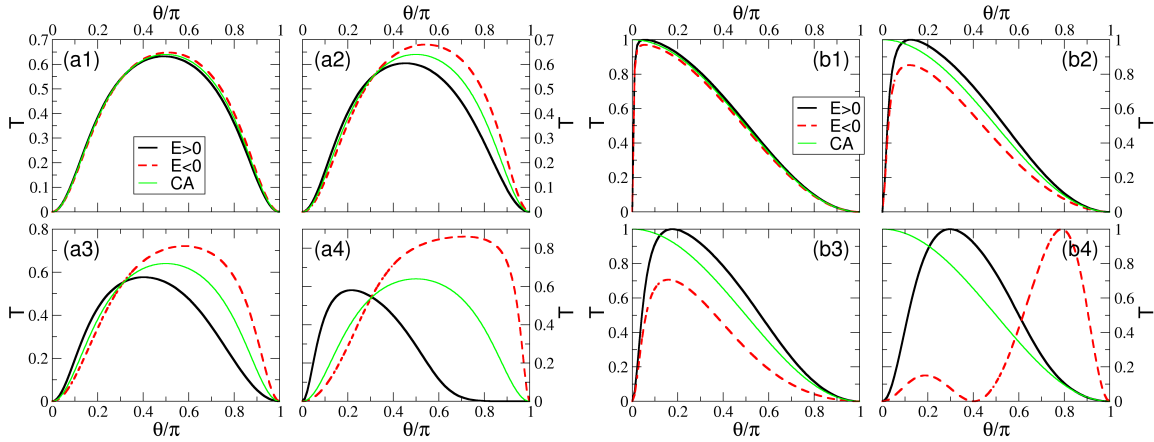


Figure 10. (Color online) Panels (a): Transmittance through the $zz(5757)$ defect line as function of the angle θ (when $\epsilon > 0$ and $-\theta$ when $\epsilon < 0$) between \mathbf{q} and the barrier. The hopping parameters at the defect have the value $\xi_a = \xi_b = \xi_c = 1$. Panels (b): Transmittance through the $zz(558)$ defect line as function of the angle θ (when $\epsilon > 0$ and $-\theta$ when $\epsilon < 0$) between \mathbf{q} and the barrier. The hopping parameters at the defect are $\xi_1 = \xi_2 = 1$. In each group of panels, the transmittance is plotted for several different energy modulus. These are: (a1) and (b1) $|\epsilon/t| = 0.01$; (a2) and (b2) $|\epsilon/t| = 0.05$; (a3) and (b3) $|\epsilon/t| = 0.1$; (a4) and (b4) $|\epsilon/t| = 0.3$. Positive energies are represented by the black full lines, while the negative ones are represented by the dashed red lines. The green full lines stand for the continuum low-energy result (that is energy-independent) as obtained in Ref. [16]. Only the curves associated with the Dirac point \mathbf{K}_+ are represented. Those for the Dirac point \mathbf{K}_- are obtained from the former by a reflection of these over the axis $\theta = \pi/2$.

parameters. As before, this feature is more easily interpreted in the continuum low-energy description of these systems [verify the good accordance between the TB and the low-energy description of these systems in Fig. 10(a1) and (b1)].

As stated in Appendix E, in the continuum low-energy limit, both the $zz(558)$ and the $zz(5757)$ defect lines can be viewed as a strip with a general potential which has $V_s \neq 0 \neq V_x$ and $V_y = 0 = V_z$ [see Eqs. (E.13) and Eqs. (E.15)]. We argued, at the end of section 3.5, concerning the *pentagon-only* defect, that perfect transmission occurs when the spin directions of the incident and transmitted waves coincide. This interpretation can be carried over the $zz(558)$ and $zz(5757)$ defects.

In the case of a $zz(558)$ defect line with hopping parameters $\xi_1 = \xi_2 = 1$ [see Figs. 10(b)], the angle of perfect transmission is $\tilde{\alpha} = \arccos(\xi_2/\xi_1^2)$ (see Appendix E); for hopping parameters $\xi_1 = \xi_2 = 1$ we obtain $\tilde{\alpha} = 0$, in accordance with what one can see in Fig. 10(b1). The fermions incident on the defect line with an angle $\theta \approx 0$ [and thus, a spin oriented along this direction] have their spin oriented in the same direction as those propagating inside the strip. Therefore, they will be perfectly transmitted, and all the others will be partly reflected.

Similarly, for a $zz(5757)$ defect line with $\xi_a = \xi_b = \xi_c = 1$, there is no angle with perfect transmission, since $\bar{\alpha} = \arccos[-(a+c)/2d]$ [see Appendix E] is not a real number when $\xi_a = \xi_b = \xi_c = 1$ [in accordance with what one can see in Fig. 10(a1)]. Inside the

strip, the spin of the fermions has a component in the z -plane, and thus will never be totally aligned with the spin of any fermion incident on the defect line.

5. Conclusions

In this paper we have presented a procedure to work out the electronic scattering either from a defect in a one-dimensional crystal, or from a periodic extended defect in two-dimensional crystals, which can be reduced to a quasi-one-dimensional tight-binding model. The formalism developed only uses simple tight-binding concepts, which reduce the scattering problem to a set of matrix manipulations. These can be easily worked out by any computational algebraic calculator.

We have illustrated the presented procedure in the context of the first neighbor tight-binding model of graphene when a defect line is oriented along the zigzag direction in an otherwise perfect crystal. Three distinct defects were studied: the *pentagon-only*, the $zz(5757)$, and the $zz(558)$ defect lines.

The latter two defect lines forced a duplication of the unit cell along the defect direction (relatively to the case of *pentagon-only* defect line). Such duplication renders the mathematical treatment of the problem more complex, by introducing an additional pair of scattering modes. These latter modes happen to be propagating at high energy around the Dirac points. Thus, for low-energy scattering processes they will be evanescent states.

All the three defect lines studied have different behaviors that strongly depend on the particular values of the hopping parameters at the defect lines. Moreover, in a companion paper [16] we treat these same problems in the continuum low-energy limit using the Dirac equation. We have shown that we can recover the low energy results from the tight-binding approach, as it should be the case.

Noteworthy is the fact that the present procedure can be used to treat more realistic extended periodic defects, that do not need to be linear. In principle, such kind of extended defects will force a considerable increase in the size of the unit cell, thus introducing a larger number of scattering modes. This, of course, renders the problem a more difficult one.

Appendix A. Left and right eigenvectors of the transfer matrix \mathbb{T}

The right eigenvectors of a non-hermitian matrix \mathbb{T} , are defined by the equation

$$\mathbb{T} |\psi_i\rangle = \lambda_i |\psi_i\rangle, \quad (\text{A.1})$$

while the left ones, are defined by

$$\langle \tilde{\psi}_i | \mathbb{T} = \lambda_i \langle \tilde{\psi}_i |. \quad (\text{A.2})$$

It is straightforward to demonstrate that, apart from a normalization constant, $C_i = \sqrt{\langle \tilde{\psi}_i | \psi_i \rangle}$, they form a dual basis. Explicitly,

$$\langle \tilde{\psi}_j | \mathbb{T} | \psi_i \rangle = \lambda_j \langle \tilde{\psi}_j | \psi_i \rangle = \lambda_i \langle \tilde{\psi}_j | \psi_i \rangle, \quad (\text{A.3})$$

and then, if $\lambda_i \neq \lambda_j$, we must have $\langle \tilde{\psi}_j | \psi_i \rangle = 0$. If we define $|\varphi_i\rangle \equiv |\psi_i\rangle/C_i$ and $|\tilde{\varphi}_i\rangle \equiv |\tilde{\psi}_i\rangle/C_i$, we can thus write

$$\langle \tilde{\varphi}_j | \varphi_i \rangle = \delta_{ij}. \quad (\text{A.4})$$

Let us now show that the left eigenvectors of a non-hermitian matrix, \mathbb{T} , are the right eigenvectors of its transpose, \mathbb{T}^T . If we take the hermitian conjugate of Eq. (A.2), we obtain

$$\mathbb{T}^\dagger |\tilde{\psi}_i\rangle = \lambda_i^* |\tilde{\psi}_i\rangle. \quad (\text{A.5})$$

Spelling out this equation in components, and taking the complex conjugate, we obtain

$$(\mathbb{T}^T)_{\alpha\beta} (|\tilde{\psi}_i\rangle)_\beta^* = \lambda_i (|\tilde{\psi}_i\rangle)_\alpha^*, \quad (\text{A.6})$$

which gives us the components of the row vector $\langle \tilde{\psi}_j |_\alpha = (|\tilde{\psi}_i\rangle)_\alpha^*$.

Appendix B. The conserved current along the 1D chain

In this appendix we are going to compute the conserved current along a quasi-one-dimensional chain. We start by doing it for a general case (using the formalism of Section 2). Later, we write the conserved current for the one-dimensional chains arising from the Fourier transformation of both the graphene layer with a *pentagon-only* defect line, and that with a *zz(5757)* [or a *zz(558)*] defect line.

The bulk TB equations of the general quasi-one-dimensional chain, Eq. (1), can be rewritten in the following manner

$$\epsilon \mathbf{c}(n) = V_L^\dagger \mathbf{c}(n-1) + H_r \mathbf{c}(n) + V_L \mathbf{c}(n+1). \quad (\text{B.1})$$

where we have used $V_R = V_L^\dagger$ (Hamiltonian hermiticity). The time-dependent counterpart of this equation can be written as

$$i\hbar \frac{\partial}{\partial t} \mathbf{c}(n, t) = V_L^\dagger \mathbf{c}(n-1, t) + H_r \mathbf{c}(n, t) + V_L \mathbf{c}(n+1, t). \quad (\text{B.2})$$

The adjoint of Eq. (B.2) reads

$$-i\hbar \frac{\partial}{\partial t} \mathbf{c}^\dagger(n, t) = \mathbf{c}^\dagger(n-1, t) V_L + \mathbf{c}^\dagger(n, t) H_r + \mathbf{c}^\dagger(n+1, t) V_L^\dagger, \quad (\text{B.3})$$

where $H_r^\dagger = H_r$ from the TB Hamiltonian hermiticity property. Given this, we can write

$$\frac{\partial}{\partial t} \mathbf{c}^\dagger(n, t) \mathbf{c}(n, t) = - \left[\mathcal{J}(n, t) - \mathcal{J}(n-1, t) \right], \quad (\text{B.4})$$

where

$$\mathcal{J}(n, t) = \frac{i}{\hbar} \left[\mathbf{c}^\dagger(n, t) V_L \mathbf{c}(n+1, t) - \mathbf{c}^\dagger(n+1, t) V_L^\dagger \mathbf{c}(n, t) \right], \quad (\text{B.5})$$

can be interpreted as the particle current along the one-dimensional chain flowing from position n to position $n+1$. If we have a stationary state of an *AB*-like chain, we can use the transfer matrix relation [see Eq. (3)] and write the conserved current as

$$\mathcal{J}(n) = \mathbf{c}^\dagger(n) \left[\frac{i}{\hbar} \left(V_L \mathbb{T} - \mathbb{T}^\dagger V_L^\dagger \right) \right] \mathbf{c}(n). \quad (\text{B.6})$$

We can further rewrite the conserved current expression using the fact that Bloch modes are the eigenvectors of the transfer matrix, $\mathbb{T}\psi_\lambda = \lambda\psi_\lambda$. Therefore, for a Bloch solution labeled by λ , whose eigenvector is ψ_λ , the conserved current reads

$$\mathcal{J}_\lambda = \psi_\lambda^\dagger \left[\frac{i}{\hbar} \left(\lambda V_L - \lambda^* V_L^\dagger \right) \right] \psi_\lambda. \quad (\text{B.7})$$

For the case of the *pentagon-only* defect line it can be inferred from Eqs. (21) that the matrix V_L reads

$$V_L = -t \begin{bmatrix} 0 & 0 \\ 1 + e^{ik_x a} & 0 \end{bmatrix}, \quad (\text{B.8})$$

while the transfer matrix is given by Eq. (24). As a consequence, we can easily conclude that the conserved current operator along the one-dimensional chain (originated from the Fourier transformation of pristine graphene along the direction of \mathbf{u}_1), is given by

$$\hat{\mathcal{J}} = \frac{i}{\hbar} \left(V_L \mathbb{T} - \mathbb{T}^\dagger V_L^\dagger \right) = \frac{t}{\hbar} \sigma_y, \quad (\text{B.9})$$

where σ_y is the y -Pauli matrix. As a consequence, the conserved current reads

$$\mathcal{J}_\lambda = \frac{t}{\hbar} \psi_\lambda^\dagger \sigma_y \psi_\lambda. \quad (\text{B.10})$$

Note that in the context of the two-dimensional graphene lattice, the above conserved current is a current directed along \mathbf{u}_2 . Therefore, the current along the y -direction is given by $\mathcal{J}_y(\lambda) = \mathcal{J}_\lambda \sqrt{3}/2$, which is in accordance with the low-energy result.

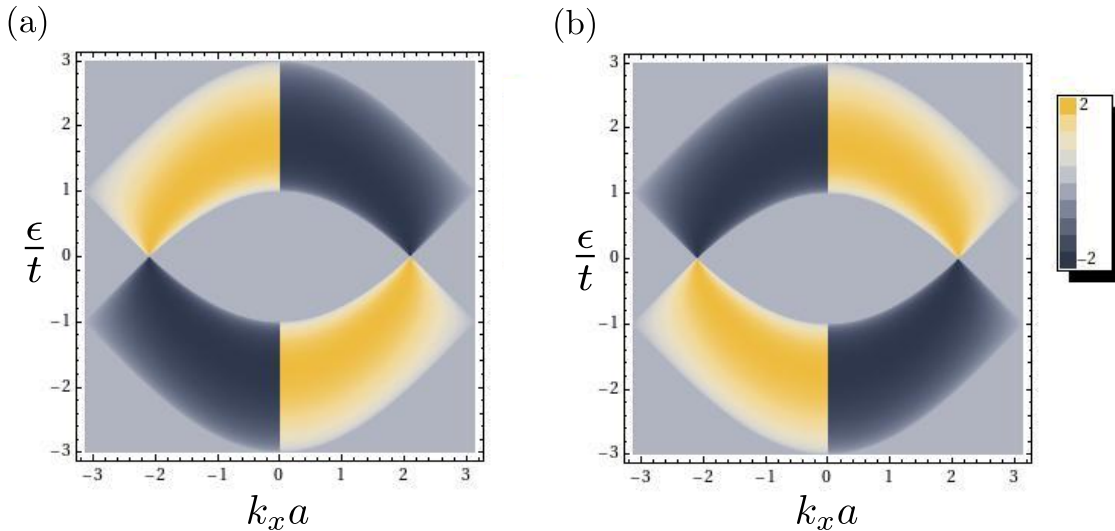


Figure B1. (Color online) Panels (a) and (b) are density plots of the current associated with the modes of the transfer matrix of the pristine graphene lattice. In accordance with the definition of sub-Section 3.4, panel (a) gives the current associated with the mode $|\Psi_\rangle$, while panel (b) gives the current associated with the mode $|\Psi_\rangle$.

In Fig. B1 we present a density plot of the current associated with each one of the modes of the transfer matrix of pristine graphene.

Similarly, for a one-dimensional chain obtained from the Fourier transform of graphene with a doubled unit cell in the direction \mathbf{u}_1 [which happens in the cases of the $zz(5757)$ and $zz(558)$ defect lines], we can infer from the bulk equations, Eqs. (39), that the matrix V_L reads

$$V_L = -t \begin{bmatrix} 0 & 0 & 0 & 0 \\ 1 & 0 & 1 & 0 \\ 0 & 0 & 0 & 0 \\ e^{i2k_x a} & 0 & 1 & 0 \end{bmatrix}, \quad (\text{B.11})$$

while the transfer matrix for this quasi-one-dimensional chain is given by Eq. (41). As a consequence, we can readily conclude that the conserved current operator along this chain, is given by

$$\hat{\mathcal{J}} = \frac{i}{\hbar} (V_L \mathbb{T} - \mathbb{T}^\dagger V_L^\dagger) = \frac{t}{\hbar} \begin{bmatrix} \sigma_y & 0_2 \\ 0_2 & \sigma_y \end{bmatrix}, \quad (\text{B.12})$$

where σ_y stands for the y -Pauli matrix, while 0_2 represents a 2×2 zero matrix. Note that the appearance of two copies of pristine graphene conserved current was to be expected because, as was already referred, the folding of the FBZ due to the duplication of the unit cell along the direction of \mathbf{u}_1 brings an additional pair of modes into the folded Brillouin zone. Both the modes associated with the $+$ and the $-$ energy sector were already known to have a current operator given by Eq. (B.9).

In Fig. B2 we present a density plot of the particle current associated with each one of the modes of the transfer matrix of graphene with a doubled unit cell along the direction of \mathbf{u}_1 .

Appendix C. The basis uncoupling the high and low-energy modes

As we have argued in the main text it is, in some circumstances, required to work with a doubled unit cell. That is, for instance, the case when treating the $zz(5757)$ and the $zz(558)$ defect lines in graphene.

With either of these two defect lines present, \mathbf{u}_1 is no longer a lattice translation. To accommodate this, it is convenient to describe pristine graphene with a unit lattice defined by the vectors $2\mathbf{u}_1$ and \mathbf{u}_2 , instead of the usual choice, \mathbf{u}_1 and \mathbf{u}_2 . The corresponding reciprocal lattice vectors will then be $\mathbf{v}_1/2$ and \mathbf{v}_2 , instead of those associated to the FBZ of pristine graphene, $\mathbf{v}_1 = 2\pi/a(1, 1/\sqrt{3})$ and $\mathbf{v}_2 = 2\pi/a(0, 2/\sqrt{3})$. Therefore, the doubling of the unit cell will have as its main consequence the folding of the FBZ along the direction of \mathbf{v}_1 [compare both panels of Fig. 8].

There will thus be twice as many atoms in the doubled unit cell as those contained in the pristine graphene one [two atoms of sub-lattice A (A_1, A_2) and two atoms of sub-lattice B (B_1, B_2)]. At the same time, there will be twice as many energy bands in the folded FBZ as those present in the pristine graphene one. Moreover, the Dirac points will now be located at $\mathbf{K}_\nu = \nu\pi/3(1/a, -\sqrt{3}/a)$ (see Fig. 8). Near the *new* Dirac points, two of the four energy bands present in the folded FBZ are the two low-energy

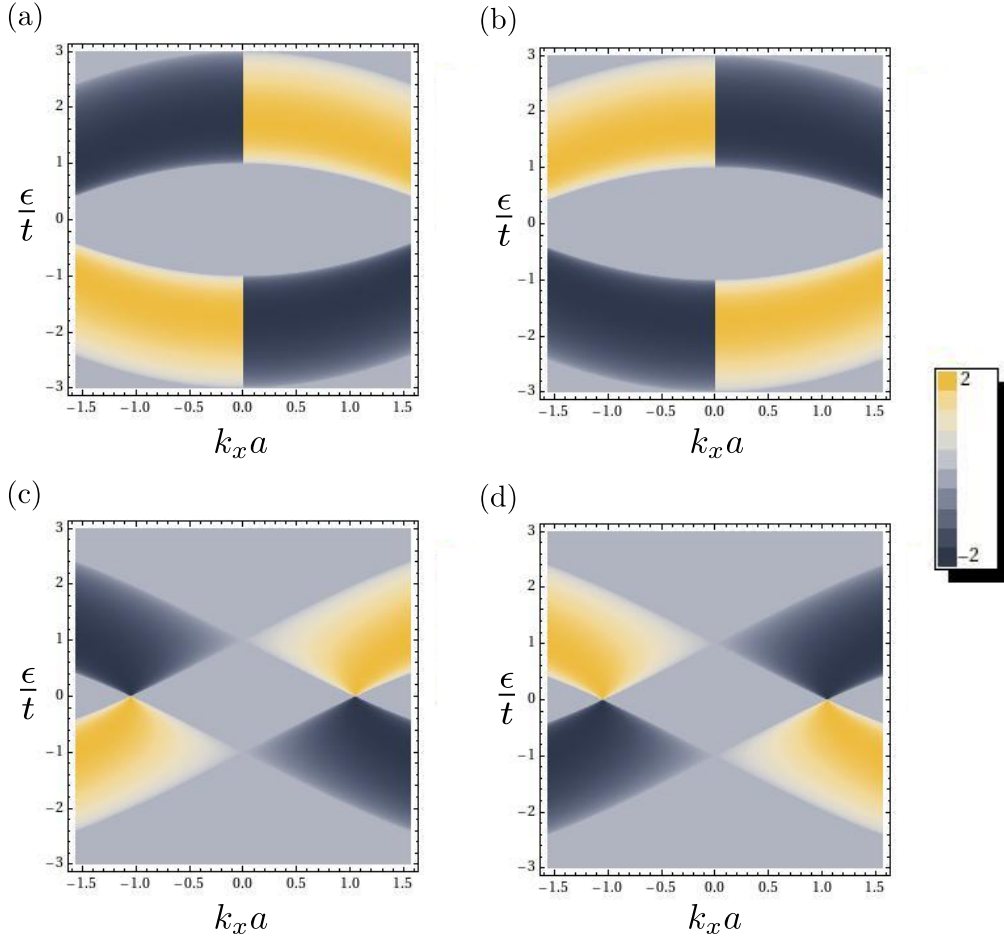


Figure B2. (Color online) Panels (a)-(d) are density plots of the current associated with the modes of the transfer matrix of the graphene lattice doubled along the \mathbf{u}_1 direction. In accordance with the definition of sub-Section 4.5, panel (a) [(b)] gives the current associated with the (+) modes, while panel (c) [(d)] gives the current associated with the (-) modes.

Dirac cones, while the other two bands are the high-energy bands [16, 19]. In what follows, we identify the two bands of low-energy near the Dirac points by $-$, while the high-energy ones are identified by $+$.

The bulk physics of graphene with a doubled unit cell must be exactly the same as that of pristine graphene. In fact, the Bloch vectors \mathbf{q} and $\mathbf{q} + \mathbf{v}_1/2$ identifying two different Bloch wave solutions in the *unfolded* Brillouin zone of pristine graphene correspond to a single Bloch vector \mathbf{q} in the folded zone. As a consequence, in the case of graphene with a doubled unit cell it is natural to expect that we can find a basis in which we can uncouple the physics associated with each one of the two Bloch solutions of the *unfolded* system: that identified by the Bloch vector \mathbf{q} and that identified by the Bloch vector $\mathbf{q} + \mathbf{v}_1/2$.

Let us then put ourselves at the wave vector $\mathbf{k} = \mathbf{q}$, where \mathbf{q} is close to the Dirac point of the folded Brillouin zone. Bloch theorem in the *unfolded* pristine graphene

allows us to write the following relations between amplitudes of the doubled unit cell:

$$A_2 = e^{i\mathbf{q}\cdot\mathbf{u}_1} A_1 = e^{iq_x a} A_1, \quad (\text{C.1a})$$

$$B_2 = e^{i\mathbf{q}\cdot\mathbf{u}_1} B_1 = e^{iq_x a} B_1. \quad (\text{C.1b})$$

Similarly, for the wave vector $\mathbf{k} = \mathbf{q} + \mathbf{v}_1/2$, we have the relations

$$A_2 = e^{i(\mathbf{q} + \frac{\mathbf{v}_1}{2})\cdot\mathbf{u}_1} A_1 = -e^{iq_x a} A_1, \quad (\text{C.2a})$$

$$B_2 = e^{i(\mathbf{q} + \frac{\mathbf{v}_1}{2})\cdot\mathbf{u}_1} B_1 = -e^{iq_x a} B_1. \quad (\text{C.2b})$$

We note that the vector $\mathbf{q} + \mathbf{v}_1/2$ can be close to the Dirac point of the unfolded zone. In fact, if we choose $\mathbf{q} = \mathbf{K}_D = (\pi/3a, -\pi/\sqrt{3}a)$, the Dirac point of the folded zone, $\mathbf{q} + \mathbf{v}_1/2 = (4\pi/3a, 0)$, the Dirac point of the unfolded zone. Then, in the unfolded zone, the state with $\mathbf{k} = \mathbf{q}$ corresponds to a high energy state (+), whereas the state $\mathbf{k} = \mathbf{q} + \mathbf{v}_1/2$ corresponds to a low energy state (-). This analysis motivates the past definitions of high and low energy modes.

As said above, we want to construct a basis that uncouples the modes originating at the two different locations of pristine graphene's FBZ: $\mathbf{k} = \mathbf{q}$ and $\mathbf{k} = \mathbf{q} + \mathbf{v}_1/2$. Equivalently, we want to construct a basis that verifies $A_+ \neq 0$, $B_+ \neq 0$ and $A_- = B_- = 0$ when $\mathbf{k} = \mathbf{q}$, as well as, $A_+ = B_+ = 0$, $A_- \neq 0$ and $B_- \neq 0$ when $\mathbf{k} = \mathbf{q} + \mathbf{v}_1/2$. Given this, we define the new basis as

$$A_+ = \frac{1}{\sqrt{2}}(A_1 + e^{-iq_x a} A_2), \quad (\text{C.3a})$$

$$B_+ = \frac{1}{\sqrt{2}}(A_1 + e^{-iq_x a} B_2), \quad (\text{C.3b})$$

$$A_- = \frac{1}{\sqrt{2}}(A_1 - e^{-iq_x a} A_2), \quad (\text{C.3c})$$

$$B_- = \frac{1}{\sqrt{2}}(A_1 - e^{-iq_x a} B_2). \quad (\text{C.3d})$$

which verifies the previous conditions. This new basis uncouples the (+) and the (-) energy sectors of the doubled unit cell. Note that the new basis written in Eqs. (C.3) is exactly the same as that defined in Eqs. (42) and (43).

Appendix D. The Dirac angle θ

In the main text the transmittance is given in terms of ϵ and $\phi = k_x a$. On the other hand, in the figures appearing in the main text the transmittance is given as function of ϵ and θ [see. Fig. D1 for the definition of θ]. We show now how given ϵ and ϕ we can obtain θ . We consider the case of a doubled unit cell.

For a doubled unit cell Schrödinger's equation reads

$$E \begin{bmatrix} A_1 \\ B_1 \\ A_2 \\ B_2 \end{bmatrix} = \begin{bmatrix} 0 & t_1 & 0 & t_2 \\ t_1^* & 0 & -te^{i\mathbf{k}\cdot\mathbf{u}_2} & 0 \\ 0 & -te^{-i\mathbf{k}\cdot\mathbf{u}_2} & 0 & t_1 \\ t_2^* & 0 & t_1^* & 0 \end{bmatrix} \begin{bmatrix} A_1 \\ B_1 \\ A_2 \\ B_2 \end{bmatrix}, \quad (\text{D.1})$$

where

$$t_1 = -t(1 + e^{-i\mathbf{k}\cdot\mathbf{u}_2}), \quad (\text{D.2})$$

$$t_2 = -te^{-2i\phi}e^{-i\mathbf{k}\cdot\mathbf{u}_2} \quad (\text{D.3})$$

Transforming the Hamiltonian to the block diagonal basis we obtain

$$E \begin{bmatrix} A_+ \\ B_+ \\ A_- \\ B_- \end{bmatrix} = \begin{bmatrix} 0 & t_+ & 0 & 0 \\ t_+^* & 0 & 0 & 0 \\ 0 & 0 & 0 & t_- \\ 0 & 0 & t_-^* & 0 \end{bmatrix} \begin{bmatrix} A_+ \\ B_+ \\ A_- \\ B_- \end{bmatrix}, \quad (\text{D.4})$$

where

$$t_+ = -t(1 + e^{-i\mathbf{k}\cdot\mathbf{u}_2} + e^{-i(\mathbf{k}\cdot\mathbf{u}_2+\phi)}), \quad (\text{D.5})$$

$$t_- = -t(1 + e^{-i\mathbf{k}\cdot\mathbf{u}_2} - e^{-i(\mathbf{k}\cdot\mathbf{u}_2+\phi)}). \quad (\text{D.6})$$

We can find a set of momentum values where t_- is equal to zero. This corresponds to the new position of the Dirac points in the new Brillouin zone. The quantity t_- can be written as

$$\begin{aligned} t_- &= -t(1 + e^{-i(\sqrt{3}k_y a/2 - \phi/2)} - e^{-i(\sqrt{3}k_y a/2 + \phi/2)}) \\ &= -t\left(1 + 2ie^{-i\sqrt{3}k_y a/2} \sin \frac{k_x a}{2}\right). \end{aligned} \quad (\text{D.7})$$

If $\sin(k_x a/2) = \pm 1/2$ and $e^{-i\sqrt{3}k_y a/2} = \pm i$ we have $t_- = 0$ (and $t_+ = -2t$). This implies

$$k_x a = \pm \frac{\pi}{3}, \quad (\text{D.8})$$

$$k_y a = \mp \frac{\pi}{\sqrt{3}}. \quad (\text{D.9})$$

Thus, the new Dirac points are located at

$$\mathbf{K}_D = \left(\pm \frac{\pi}{3a}, \mp \frac{\pi}{\sqrt{3}a} \right). \quad (\text{D.10})$$

The Dirac angle θ is defined as in Fig. D1.

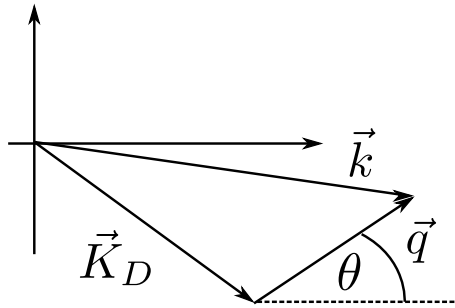


Figure D1. (color online) Definition of the Dirac angle $\theta \in [0, \pi]$.

The dispersion of the low energy modes reads

$$\epsilon^2 = |t_-|^2/t^2 = 1 + 4\sin^2 \frac{\phi}{2} + 4\sin \frac{\phi}{2} \sin \frac{k_y \sqrt{3}a}{2}. \quad (\text{D.11})$$

The largest and the smallest value of $\phi = ak_x$ are given when $k_y = K_{Dy}$. In this case

$$\epsilon^2 = (1 - 2 \sin \frac{\phi}{2})^2 \Rightarrow \sin \frac{\phi}{2} = \frac{1 \pm \epsilon}{2}. \quad (\text{D.12})$$

Then

$$\phi_{min} = 2 \arcsin \frac{1 - \epsilon}{2}, \quad (\text{D.13})$$

and

$$\phi_{max} = 2 \arcsin \frac{1 + \epsilon}{2}. \quad (\text{D.14})$$

The coordinate $k_y a$ is given by

$$k_y a = \frac{2}{\sqrt{3}} \arcsin \frac{\epsilon^2 - 4 \sin^2 \frac{\phi}{2} - 1}{4 \sin \frac{\phi}{2}}. \quad (\text{D.15})$$

Since $\mathbf{k} = \mathbf{K}_D + \mathbf{q}$ we have

$$q_x = k_x - K_{Dx} = k_x - \frac{\pi}{3a}, \quad (\text{D.16})$$

$$q_y = k_y - K_{Dy} = k_y + \frac{\pi}{a\sqrt{3}}. \quad (\text{D.17})$$

From Fig. D1 is clear that

$$\theta = \arccos \frac{q_x}{\sqrt{q_y^2 + q_x^2}} = \arccos \frac{\phi - \pi/3}{\sqrt{(k_y a + \pi/\sqrt{3})^2 + (\phi - \pi/3)^2}}. \quad (\text{D.18})$$

Thus, given ϕ and ϵ we can compute $k_y a$ and θ . Scanning ϕ between ϕ_{min} and ϕ_{max} originates $\theta \in [0, \pi]$. Thus θ is a parametric function of ϕ and ϵ .

Appendix E. The continuum low-energy limit of the TB

Starting from the results of Ref. [16], in this appendix we show how can one determine the general potential governing the behavior of the fermions propagating inside the strip that describes the defect line in the continuum low-energy approximation.

As argued in Ref. [16], in the continuum low-energy limit, one can see the defect line as a "strip of width W in the y direction, where there is a general local potential $V(y) = V_s \mathbb{I} + V_x \sigma_x + V_y \sigma_y + V_z \sigma_z$ for $|y| < W/2$ ". Therefore, in that region, the Dirac Hamiltonian reads

$$H = \hbar v_F (\nu \sigma_x (-i \partial_x) + \sigma_y (-i \partial_y)) + (V_s \mathbb{I} + \mathbf{V} \cdot \boldsymbol{\sigma}). \quad (\text{E.1})$$

Taking the continuum low-energy limit of such a system, is equivalent, either to take the limit $W \times (V_s, \mathbf{V}) \rightarrow (v_s, \mathbf{v})$ when $W \rightarrow 0$ keeping ϵ and q_x finite, or to take the limit $\epsilon, q_x \rightarrow 0$ keeping W finite.

In either case, one can write a boundary condition matrix, \mathcal{M} , relating the wavefunction at each side of the defect line, $\Psi(x, W/2) = \mathcal{M} \Psi(x, -W/2)$. In general it reads [16]

$$\mathcal{M} = e^{-i \sigma_y (v_s \mathbb{I} + \mathbf{v} \cdot \boldsymbol{\sigma}) / v_F}, \quad (\text{E.2})$$

where $\boldsymbol{\sigma} = (\sigma_x, \sigma_y, \sigma_z)$ stand for the Pauli matrices, while v_F is the Fermi velocity.

Defining $\alpha := \sqrt{v_s^2 - (v_x^2 + v_z^2)}/v_F\hbar$, and using $\sigma_i\sigma_j = \delta_{ij}i\epsilon_{ijk}\sigma_k$, it is simple to show that

$$\mathcal{M} = e^{-iv_y/\hbar v_F} \begin{pmatrix} \cos \alpha - \frac{v_x}{\hbar v_F \alpha} \sin \alpha & \frac{v_z - v_s}{\hbar v_F \alpha} \sin \alpha \\ \frac{v_z + v_s}{\hbar v_F \alpha} \sin \alpha & \cos \alpha + \frac{v_x}{\hbar v_F \alpha} \sin \alpha \end{pmatrix}. \quad (\text{E.3})$$

For the *pentagon-only* defect line, the continuum low-energy boundary condition matrix, \mathcal{M}_{55} , reads [16]

$$\mathcal{M}_{55} = \begin{pmatrix} 0 & 1 \\ -1 & \xi \end{pmatrix}. \quad (\text{E.4})$$

The potential terms (V_s, \mathbf{V}) thus read

$$V_s = \frac{v_s}{W} = -\frac{\hbar v_F \alpha}{W \sin \alpha}, \quad (\text{E.5a})$$

$$V_x = \frac{v_x}{W} = \frac{\cos \alpha}{W \sin \alpha} \hbar v_F \alpha, \quad (\text{E.5b})$$

$$V_z = \frac{v_z}{W} = 0, \quad (\text{E.5c})$$

while V_y is arbitrary, and thus can be taken equal to 0. Moreover, we can do the identification

$$2 \cos \alpha = \xi. \quad (\text{E.6})$$

The term V_s , is a mass term, that only causes a shift in the energy of the massless Dirac fermion. This term will deviate the fermion's direction of propagation inside the strip when compared to its direction outside the strip. The term V_x deviates the fermion's direction of propagation and tilts its spin. The spin of the fermion will no longer be aligned along its direction of propagation as happens for fermions outside the strip.

For the sake of comparison, let one write the eigenstate associated with a free massless Dirac fermion propagating outside the strip [Eq. (E.1) with $(V_s, \mathbf{V}) = (0, \mathbf{0})$] and that of a massless fermion propagating inside the strip [Eq. (E.1) with $V_y = 0 = V_z$]. The first can be written as

$$|\psi_\nu^\gtrless\rangle = \frac{1}{\sqrt{2}} \begin{pmatrix} 1 \\ s\nu e^{\pm i\nu\theta} \end{pmatrix} e^{i(q_x x \pm q_y y)}, \quad (\text{E.7})$$

while the second reads

$$|\phi_\nu^\gtrless\rangle = \frac{1}{\sqrt{2}} \begin{pmatrix} 1 \\ \tilde{s} e^{\pm i\beta_\nu} \end{pmatrix} e^{i(\tilde{q}_x x \pm \tilde{q}_y y)}. \quad (\text{E.8})$$

In the above expressions, the symbol $>$ ($<$) identifies the state propagating to $y \rightarrow +\infty$ ($y \rightarrow -\infty$), and $\nu = \pm 1$ identifies the Dirac point \mathbf{K}_ν the eigenstate refers to. The symbol s identifies the sign of the energy of the free fermion, $s = \text{Sign}[\epsilon]$, while the angle $\theta = \arctan(q_y/q_x)$ determines the orientation of its spin. Similarly, $\tilde{s} = \text{Sign}[\epsilon - v_s]$ stands for the sign of the energy of the fermion propagating inside the strip, while

$$\beta_\nu = \arctan \left(\frac{\tilde{q}_y}{\nu \tilde{q}_x + v_x/W v_F \hbar} \right), \quad (\text{E.9})$$

determines the orientation of its spin.

The translation symmetry along the defect line, forces $\tilde{q}_x \equiv q_x = |\mathbf{q}| \cos \theta = (\epsilon/v_F \hbar) \cos \theta$. Then, \tilde{q}_y can be determined from the energy, ϵ , and the angle of incidence in the strip, θ . It reads

$$\tilde{q}_y = \sqrt{\left(\frac{\epsilon - v_s/W}{v_F \hbar}\right)^2 - \left(\frac{\nu \epsilon \cos \theta + v_x/W}{v_F \hbar}\right)^2}. \quad (\text{E.10})$$

Very near the Dirac points, $\epsilon, q_x \rightarrow 0$, all the Dirac fermions travelling inside the strip will have the same β_ν

$$\beta_\nu = \arctan\left(\frac{\sqrt{v_s^2 - v_x^2}}{v_x}\right). \quad (\text{E.11})$$

From Eqs. (E.5) and Eq. (E.11), one can easily conclude that when $\epsilon, q_x \rightarrow 0$, we have that $\alpha \equiv \beta_\nu$. Thus, in the low-energy limit, all the fermions propagating inside the strip, will have their spins aligned in the same direction. As discussed in the main text, perfect transmission occurs when $\theta = \beta_\nu$.

In a similar way, we can also compute the general potential describing both the $zz(558)$ and the $zz(5757)$ defect line in the continuum low-energy limit. The boundary condition matrix *seen* by the massless Dirac fermions at the $zz(558)$ and at the $zz(5757)$ defect lines are computed in Ref. [16]. The one originating from the $zz(558)$ defect line reads

$$\mathcal{M}_{558} = \begin{pmatrix} 0 & 1 \\ -1 & 2\frac{\xi_2}{\xi_1} \end{pmatrix}. \quad (\text{E.12})$$

This boundary condition is very similar to the one computed for the *pentagon-only* defect line, Eq. (E.4). They are equal if we define an effective hopping parameter $\tilde{\xi} := 2\xi_2/\xi_1^2$. Therefore, the corresponding general potential is going to be given by

$$V_s^{558} = \frac{v_s^{558}}{W} = -\frac{\hbar v_F \tilde{\alpha}}{W \sin \tilde{\alpha}}, \quad (\text{E.13a})$$

$$V_x^{558} = \frac{v_x^{558}}{W} = \frac{\cos \tilde{\alpha}}{W \sin \tilde{\alpha}} \hbar v_F \tilde{\alpha}, \quad (\text{E.13b})$$

$$V_y^{558} = \frac{v_y^{558}}{W} = 0 = \frac{v_z^{558}}{W} = V_z^{558}, \quad (\text{E.13c})$$

where $\tilde{\alpha} = \arccos(\xi_2/\xi_1^2)$ is the angle the spin of the fermions propagating inside the strip will make with the horizontal direction, in the limit where $\epsilon, \phi \rightarrow 0$.

From the boundary condition matrix originating from the $zz(5757)$ defect line,

$$\mathcal{M}_{5757} = \begin{pmatrix} -a/d & -b/d \\ b/d & -c/d \end{pmatrix}, \quad (\text{E.14})$$

where $a = 2\xi_c^2(\xi_b^2 - \xi_a^2/4)$, $b = -\xi_a(\xi_b^2 - \xi_a^2)$, $c = 2(\xi_b^4 + \xi_a^4 + \xi_b^2 \xi_a^2)/\xi_c^2$ and $d = 2\xi_b(\xi_b^2 + \xi_a^2/2)$, one can write the following general potential

$$V_s^{5757} = \frac{v_s^{5757}}{W} = -\frac{\hbar v_F \bar{\alpha}}{W \sin \bar{\alpha}} \frac{b}{d}, \quad (\text{E.15a})$$

$$V_x^{5757} = \frac{v_x^{5757}}{W} = \frac{\cos \bar{\alpha} + a/d}{W \sin \bar{\alpha}} \hbar v_F \bar{\alpha}, \quad (\text{E.15b})$$

$$V_y^{5757} = \frac{v_y^{5757}}{W} = 0 = \frac{v_z^{5757}}{W} = V_z^{5757}, \quad (\text{E.15c})$$

where $\bar{\alpha} = \arccos[-(a+c)/2d]$ is the angle the spin of the fermions propagating inside the strip will make with the horizontal direction, in the limit where $\epsilon, \phi \rightarrow 0$.

Acknowledgments

J. N. B. R. was supported by Fundação para a Ciência e a Tecnologia (FCT) through Grant No. SFRH/BD/44456/2008. N. M. R. P. was supported by Fundos FEDER through the Programa Operacional Factores de Competitividade - COMPETE and by FCT under project no. PEst-C/FIS/UI0607/2011. N. M. R. P. acknowledges both the hospitality and the funding from the Graphene Research Centre at the National University of Singapore, where this work was completed.

References

- [1] Peres N M R 2010 *Rev. Mod. Phys.* **82** 2673
- [2] Huang P Y, Ruiz-Vargas C S, van der Zande A M, Whitney W S, Levendorf M P, Kevek J W, Garg S, Alden J S, Hustedt C J, Zhu Y, Park J, McEuen P L and Muller D A 2011 *Nature* **469** 389
- [3] Incze P N, Yoo K J, Tapasztó L, Dobrik G, Lábár J, Horváth Z E, Hwang C and Biró L P 2011 *Appl. Phys. Lett.* **99** 023104
- [4] Yu Q, Jauregui L A, Wu W, Colby R, Tian J, Su Z, Cao H, Liu Z, Pandey D, Wei D, Chung T F, Peng P, Guisinger N, Stach E A, Bao J, Shem Pei S and Chen Y P 2011 *Nature Materials* **10** 443
- [5] Jaureguia L A, Cao H, Wud W, Yud Q and Chen Y P 2011 *Solid State Communications* **151** 1100
- [6] Yazyev O V and Louie S G 2010 *Phys. Rev. B* **81** 195420
- [7] Jiang L, Lv X and Zheng Y 2011 *Phys. Lett. A* **376** 136
- [8] Gunlycke D and White C T 2011 *Phys. Rev. Lett.* **106** 136806
- [9] Tsen A W, Brown L, Levendorf M P, Ghahari F, Huang P Y, Havener R W, Ruiz-Vargas C S, Muller D A, Kim P and Park J 2012 *Science* **336** 1143–1146
- [10] Sautet P and Joachim C 1988 *Phys. Rev. B* **38** 12238
- [11] Mizes H and Conwell E 1991 *Phys. Rev. B* **44** 3963
- [12] Peres N M R 2009 *Eur. Phys. J. B* **72** 183
- [13] Khomyakov P A, Brocks G, Karpan V, Zwierzycki M and Kelly P J 2005 *Phys. Rev. B* **72** 035450
- [14] Ando T 1991 *Phys. Rev. B* **44** 8017
- [15] Peres N M R and Sols F 2008 *J. Phys.: Condens. Matter* **20** 255207
- [16] Rodrigues J N B, Peres N M R and Lopes dos Santos J M B 2012 *Phys. Rev. B* **86** 214206
- [17] Lahiri J, Lin Y, Bozkurt P, Oleynik I I and Batzill M 2010 *Nature Nanotechnology* **5** 326
- [18] Katsnelson M I, Novoselov K S and Geim A K 2006 *Nature Physics* **2**(9) 620–625
- [19] Rodrigues J, Gonçalves P, Rodrigues N, Ribeiro R, Lopes dos Santos J M B and Peres N M R 2011 *Phys. Rev. B* **84** 155435